Department of Aerospace Engineering
The Pennsylvania State University
University Park, PA 16802

Semi-Annual Report on
NASA Grant No. NSG 1580

BROADBAND JET NOISE AMPLIFICATION BY A PURE TONE EXCITATION

Sponsored by

National Aeronautics and Space Administration

Langley Research Center
Hampton, VA 23665

Submitted by: Date:

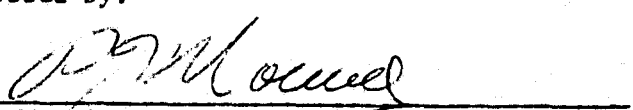

7/14/80

P. J. Morris, Principal Investigator
Associate Professor of Aerospace Engineering
233-L Hammond Building
University Park, PA 16802

(814) 863-0157

Introduction

During this phase of the program the analytical model for the amplification of broadband jet noise has been further developed and some numerical solutions have been performed. These calculations have been published [1] (attached as Appendix A). The calculations on the stability of compressible axisymmetric jets, which were described in the first annual report on this grant, have been documented and submitted for publication [2] (attached as Appendix B). The facilities, instrumentation and data processing techniques, required for the experimental part of this program are nearing completion and some preliminary measurements have been performed. It is expected, as described below, that much of the flow data, which is required to assist in the modeling of the flow will be collected during the second part of this grant. A brief discussion of the analytical and experimental parts of the program is given below.

Analysis

The present status of the calculations is described in detail in references [1] and [2] so details are not presented here. However, some general conclusions can be drawn. The numerical procedure that has been developed is definitely more flexible than previous formulations. These previous works have employed an integral analysis which requires assumptions to be made about the characteristic shapes of the mean velocity profile and the turbulent kinetic energy distribution, (see Chan [3], for example). The present work confirms that these assumptions are reasonable in the case of a single jet in a stationary ambient medium. The power of the present method lies in its ability to examine interactions in flows with more

complicated geometries. For example the present technique is readily adaptable to the problem of a single jet in a co-flowing stream with a significant boundary layer on the external surface of the nozzle. Such calculations were not possible with the integral formulation. During the second half of this year, while awaiting experimental results, work will concentrate on improving the calculation procedure. Specific attention will be paid to the initial conditions. The present calculations have assumed a mean velocity profile at the jet exit which is already developed into the similarity form of the annular mixing region. Calculations will be performed assuming a turbulent boundary layer at the jet exit. The effect of initial boundary layer thickness on the pure tone excitation of the jet will then be examined. The model proposed for the "wave-induced stresses" in the present calculations involves a scalar eddy viscosity. Until the experimental results are available no further development of this model will be attempted.

Experimental Program

The nature of the present investigation immediately introduces the concept of conditional sampling, as a way of evoking the particular portions of the flow of most interest. A review of the techniques available, as well as the specific method to be used in the present experiments is outlined below. However, it is important that the behavior of the jet flow in the mixing and self-preserving regions based on available experimental data, be investigated; in particular, the fluid dynamic concepts associated with the large scale structures. This not only helps in the understanding of

the various mechanisms involved but also places in perspective the problems that may be encountered.

Speculations about the existence of large scale structures in free shear layers developed from the two-dimensional experiments of Brown and Roshko [4]. While investigating density effects, they observed an organized coherent structure, shown on shadowgraphs, persisting downstream of the splitter phase at a Reynolds number of order 1×10^6. Winant and Browand [5] earlier showed that the vortex pairing process in a two-dimensional shear layer was a result of shear layer instability, but the Reynolds number in their experiments was quite low. Later, Dimotakis and Brown [6] investigated the existence of large structures at a Reynolds number of 3×10^6. They verified the existence of the previously observed structures and showed that there exists a periodicity to the phenomenon. However, they also showed the development of three-dimensional eddy structures and concluded that initial conditions as well as the finite extent of the apparatus play an important role. Chandrsuda et al. [7] also pointed out the three dimensional development of these structures and their sensitivity to upstream free stream turbulence.

The interesting outcome of the above work is the applicability of these ideas to noise generation in the mixing region of a jet. The question that has been posed is, whether the large scale structures are direct or indirect noise generators? In the latter case, how does the excitation of large structures in a jet result in increases in broadband jet noise radiation? The above questions are fundamental, therefore, in guiding the experimental procedures. Considerable insight, closely associated with our program, is provided from the experiments of Yule [8]. He studied the structure of the

mixing region at a Reynolds number of 2×10^5 and concluded that the observed vortex rings are only a transitional phenomenon and also that there are substantial differences between these vortex structures and the structure in the fully developed region. He established that the coherent eddies are dominating components but are far from deterministic. Although a wide range of data are available on the acoustic characteristics of excited jets, very little has been reported on the flow characteristics. A thorough explanation of the phenomenon will only be provided, however, from measurements inside the flow itself. Hussain et al. [9,10,11] have reported flow measurements, but so far they have concentrated on low excitation levels and Reynolds numbers of up to approximately 2×10^5, while Kibens et al. [12,13, 14] have concentrated on the behavior of the vortex pairing process, which appears to only occur at very low Reynolds numbers.

In our program, therefore, a major effort is being made to provide (i) detailed turbulence characteristics under excitation, (ii) a comparison with unexcited tests and (iii) a comparison with analytical models which is presently lacking.

As outlined above, a powerful tool for detecting specific flow events is conditional sampling. The use of this technique presupposes, however, certain criteria, and the choice of these criteria is a fundamental and critical process. Yule [8] after obtaining velocity time histories, chose peaks in the velocity fluctuations as the criterion. Velocity levels were also used in the experiments of Bruun [15]. In excited jets, sampling can be initiated from the forcing mechanism providing the trigger (phase-averaging) or a choice of certain level of intensity at the exit of a jet

being a fraction of the measured non-excited value [9]. A novel and powerful pattern recognition technique has been developed by Wallace et al. [16, 17]. It has been primarily applied to boundary layer flows and is a digital method utilizing a fully computerized system. Short time temporal averages are selected and criteria are based on sharp gradients of velocity and acceleration detected from digitized output signal histories. Blackwelder [18] and Wygnaski [19] also outlined concepts in pattern recognition of coherent eddies.

In the present program a number of the above ideas will be incorporated based on an overall philosophy as shown on Figure 1.

The following measurements and processing techniques will be used:

1. Velocity time histories, longitudinal and transverse under no excitation using hot wire sensors.

2. Same as (1) but under excitation.

3. Pressure signals in the near field.

4. Digitization of signals under (1), (2), and (3).

5. Search for clearly defined events such as peaks or other repeatable values.

6. Selection of the conditional sampling criteria and comparison with other established criteria detected under the same procedures above.

7. Turbulence characteristics and phase averaging of first and second order moments of the velocity.

8. Comparison of excited and unexcited cases enabling deduction of "wave induced stresses."

9. Comparison with theory.

The experimental facilities are nearing completion. The circular pipe-nozzle system has been installed as well as the traversing gear. Automatic positioning of two coordinate axes is possible, namely transverse and vertical as shown in Figure 2. For the transverse motion (x) 10,000 step-motor steps are provided per 1/2 in. and for the vertical (y) direction, 10,000 per in. Accuracy can therefore be obtained within 5×10^{-5} inches for x and 10^{-4} inches for the y direction. The motors are driven by SLO-SYN indexers, and the downstream positioning (z) is performed manually.

Manufacture of the exponential horns is complete and the exact dimensions are shown in Figure 3. Delivery of two of the four loudspeaker drivers is still pending and experiments will be conducted using only the system of two speakers. The processing instrumentation is shown in Figures 4, 5, and 6. During preliminary tests to establish the proper operation of the installed nozzle system, an exit velocity of 210 ft/sec (64 m/s) maximum was measured, yielding a flow Reynolds number of approximately 4×10^5. This value is lower than anticipated and reasons for this can be attributed to heavy losses in fan efficiency at high speeds. Considerable interference has also been encountered close to the operating facility due to other experimental rigs in the vicinity of our own. Heavy vibration loss dominated the interference resulting in contamination of the hot wire signals. Recirculating flow has also caused problems. The facility will be operated during evening hours to eliminate the external influences mentioned above. A program has been initiated for the construction and establishment of the jet facility proposed and shown in Figure 7.

It is expected that flow measurements of turbulence properties of the jet in unexcited and plane-mode excitation will be completed by September 1980 and that phase averaged measurements for the same excitation conditions will be available by the end of the grant year.

References

1. Morris, P. J.: "A model for broadband jet noise amplification," AIAA Paper 80-1004, 1980.

2. Morris, P. J.: "The viscous stability of compressible axisymmetric jets," submitted for publication in AIAA Journal.

3. Chan, Y. Y.: "Nonlinear spatial wave development in an axisymmetrical turbulent jet," NRC Aero. Rep. LR-585, Nat. Aero. Est., Ottawa, April 1975.

4. Brown, G. L. and Roshko, A.: "On density effects and large structure in turbulent mixing layers," Journal of Fluid Mechanics, Vol. 64, Pt. 4, 1974, pp. 775-816.

5. Winant, C. D. and Browand, F. K.: "Vortex pairing: The mechanism of turbulent mixing-layer growth at moderate Reynolds numbers," Journal of Fluid Mechanics, Vol. 63, Pt. 2, 1974, pp. 237-255.

6. Dimotakis, P. E. and Brown, G. L.: "The mixing layer at higher Reynolds number: Large scale structure dynamics and entrainment," Journal of Fluid Mechanics, Vol. 78, Pt. 3, 1976, pp. 535-560.

7. Chandrsuda, C., Mehta, R. D., Weir, A. D., and Bradshaw, P.: "Effect of free-stream turbulence on large structure in turbulent mixing layers," Journal of Fluid Mechanics, Vol. 85, Pt. 4, 1978, pp. 693-704.

8. Yule, A. J.: "Large scale structure in the mixing layer of a round jet," Journal of Fluid Mechanics, Vol. 89, Pt. 3, 1978, pp- 413-432.

9. Hussain, A. K. M. F. and Zaman, K. B. M. Q.: "Effect of acoustic excitation on the turbulent structure of a circular jet," Proc. of the Third Interagency Symposium in Transportation Noise, University of Utah, 1975.

10. Hussain, A. K. M. F. and Zaman, K. B. M. Q.: "Controlled perturbation of circular jets: Structure and mechanisms of turbulence I," Proc. Berlin, 1977, pp. 31-42.

11. Hussain, A. K. M. F., Kleis, S. J., and Sokolov, M.: "A turbulent spot in an axisymmetric free shear layer: Part 2," Dept. of Mechanical Engineering, University of Houston, 1979.

12. Kibens, V.: "Interaction of jet flowfield instabilities with flow system resinances," AIAA Paper 80-963, 1980.

13. Kibens, V.: "Discrete noise spectrum generated by an acoustically excited jet," AIAA Journal, Vol. 18, No. 4, April 1980, pp. 434-441.

14. Kitaplioglu, C. and Kibens, V.: "Discrete vortex modelling of an axisymmetric jet flow field," AIAA Paper 80-1003, 1980.

15. Bruun, H. H.: "A time-domain analysis of the large scale flow structure in a circular jet. Part 1, Moderate Reynolds number," Journal of Fluid Mechanics, Vol. 83, Pt. 4, 1977, pp. 641-671.

16. Wallace, J. M., Bodkey, R. S., Eckelman, H.: "Pattern recognized structures in bounded turbulent shear flows," Vol. 83, Pt. 4, 1977, pp. 673-693.

17. Eckelman, H., Wallace, J. M., Brodkey, R. S.: "Pattern recognition, a means for detection of coherent structures in bounded turbulent shear flows," Proc. of the Dynamic Flow Conference, Denmark, 1978, pp. 161-172.

18. Blackwelder, R. F.: "Pattern recognition of coherent eddies," Proc. of dynamic flow conference, Denmark, 1978, pp. 173-190.

19. Wygnaski, I.: "The recognition of an evoked large scale structure in turbulent shear flows," Proc. of the Dynamic Flow Conference, Denmark, 1978, pp. 191-211.

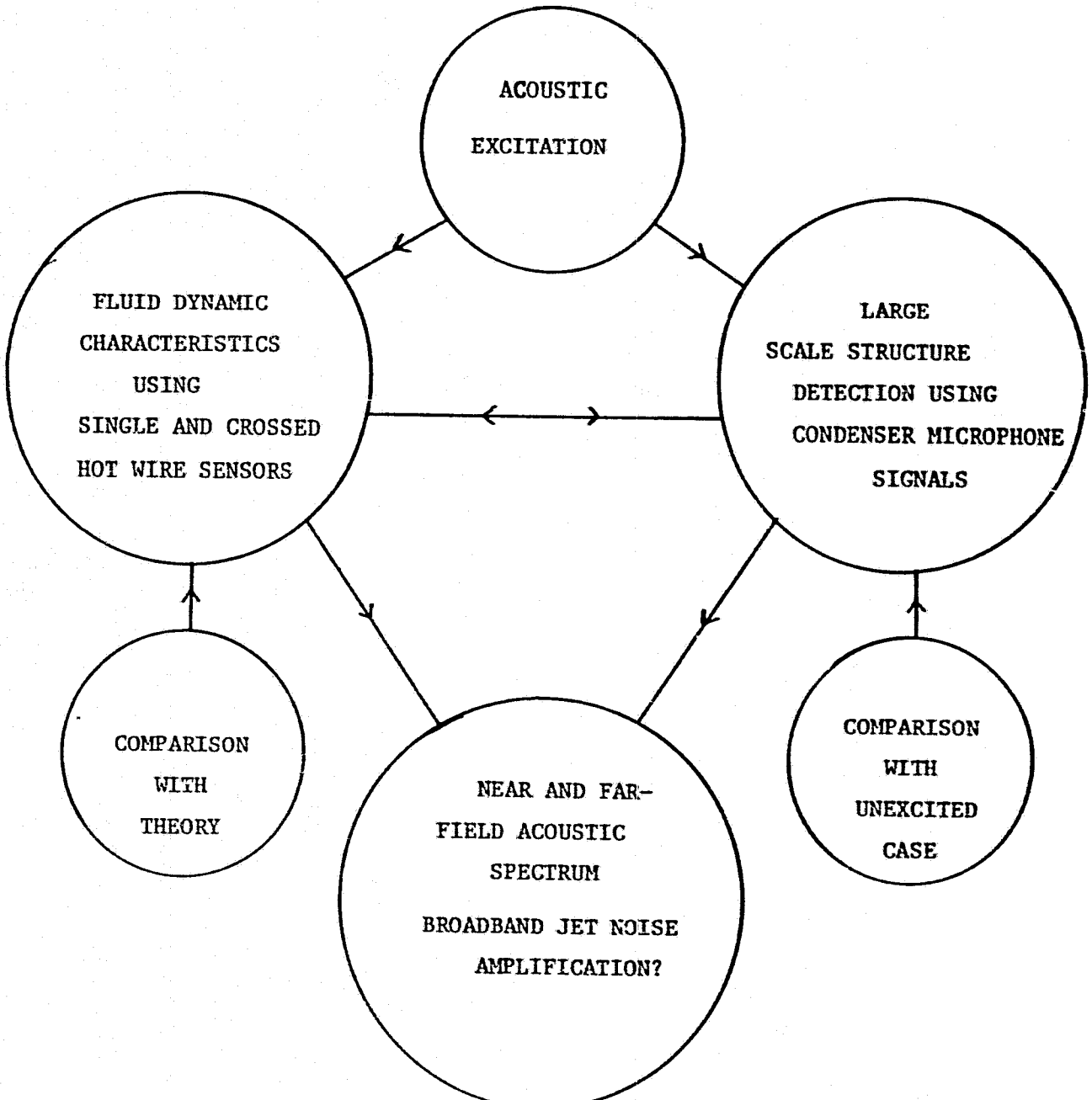

FIGURE 1 : Experimental Philosophy

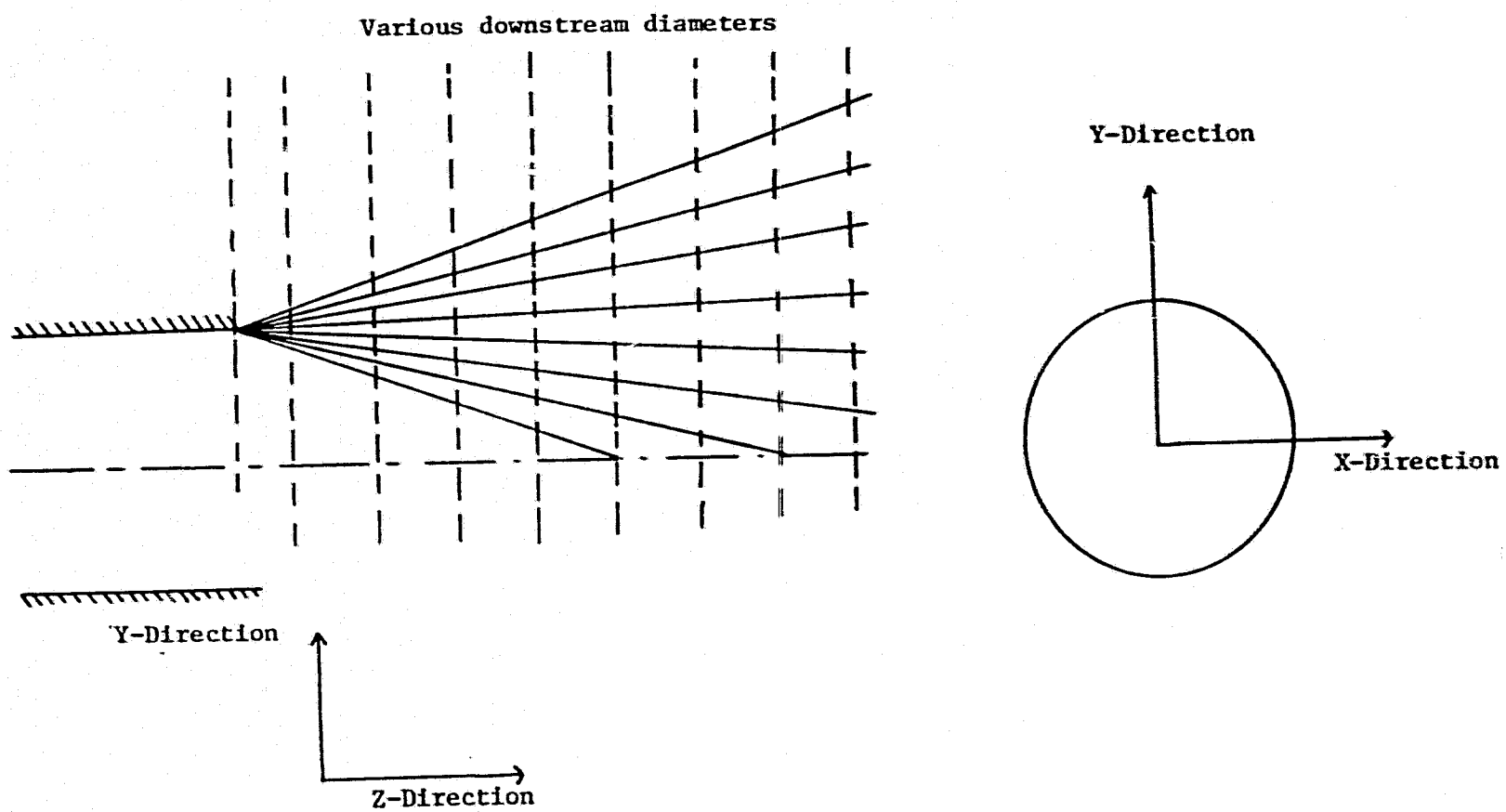

FIGURE 2 : Coordinate System and Measuring Area

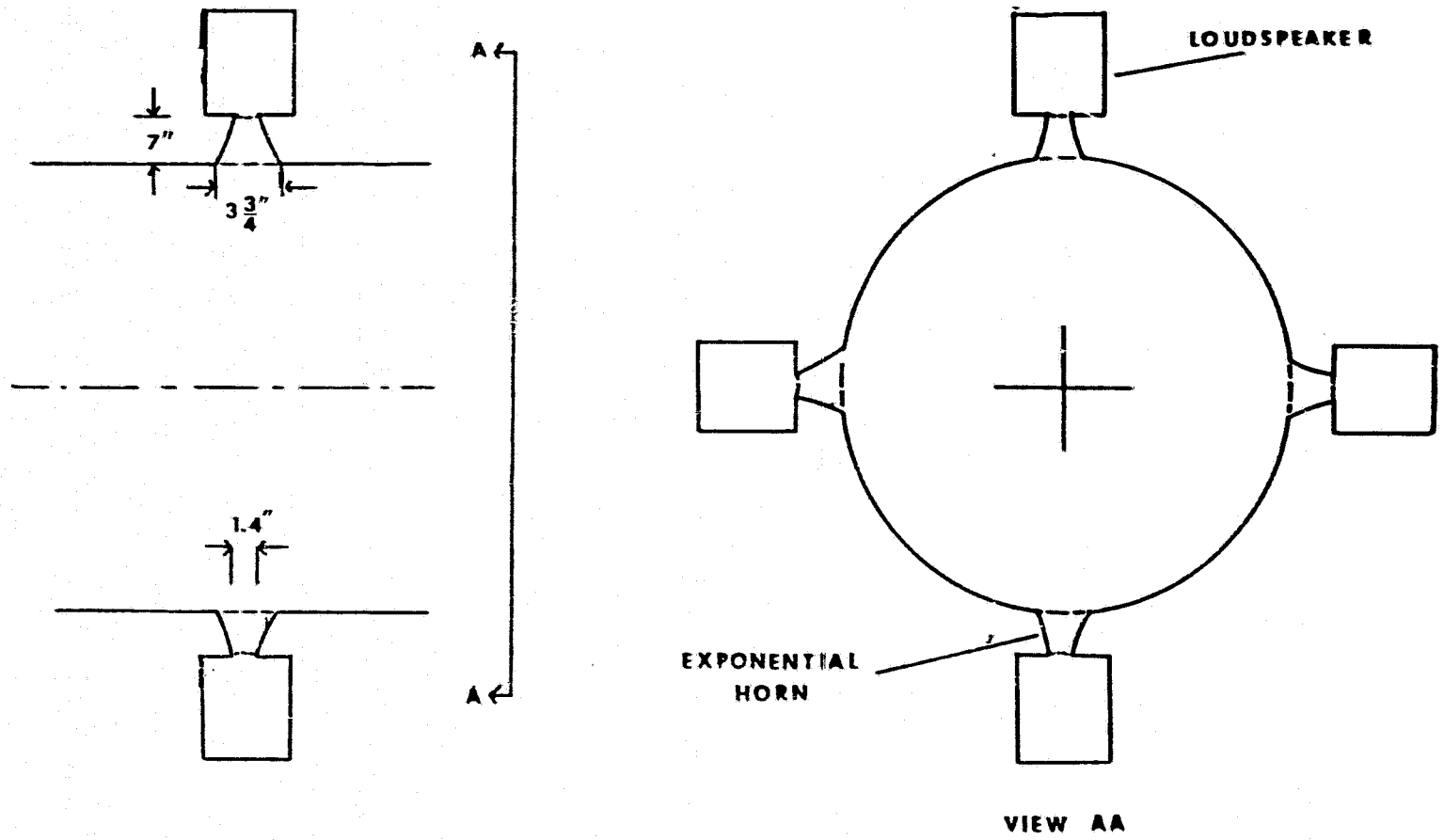

FIGURE 3 – ACOUSTIC EXCITATION SYSTEM

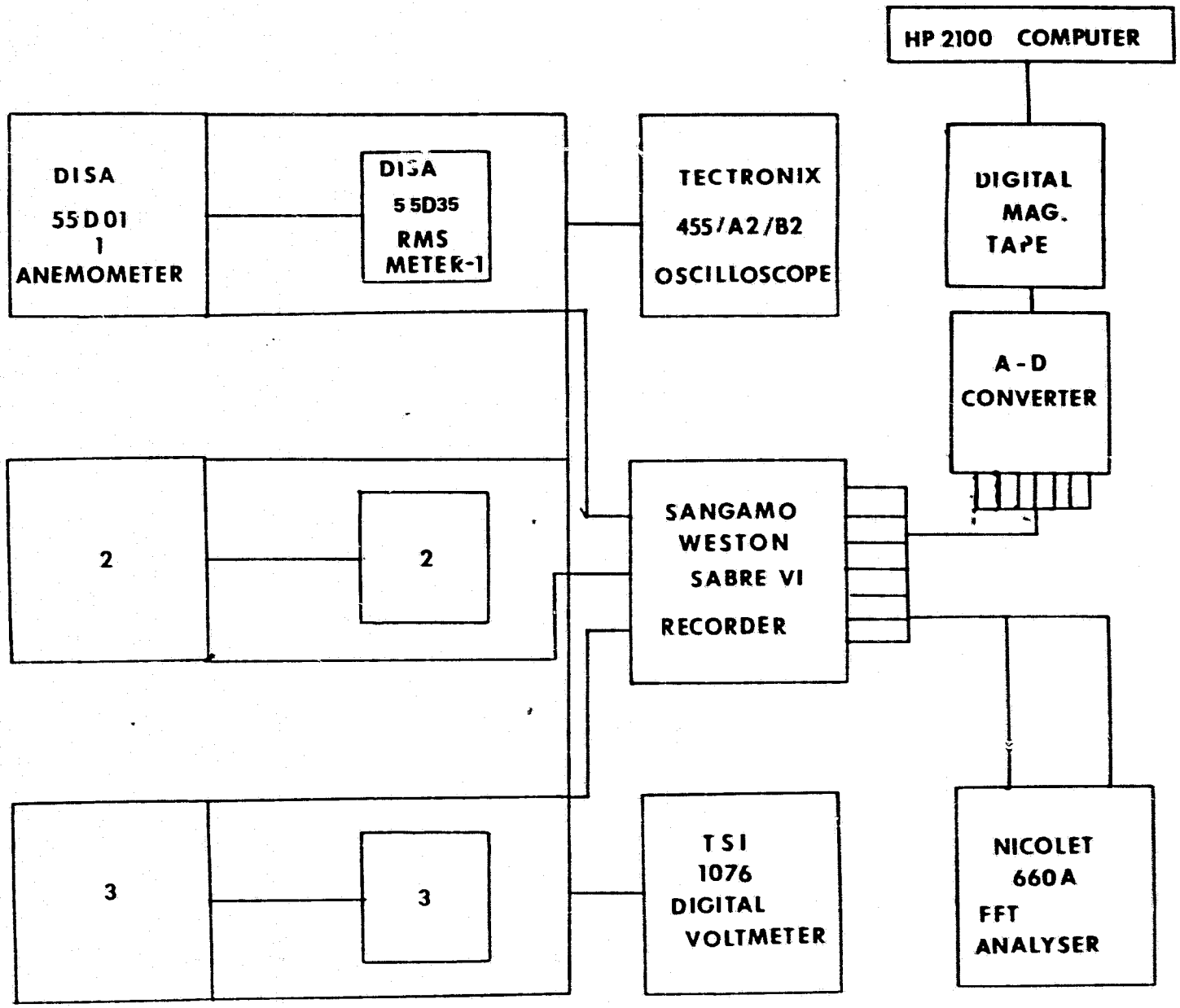

FIGURE 4 : Instrumentation for Fluid Dynamic Measurements

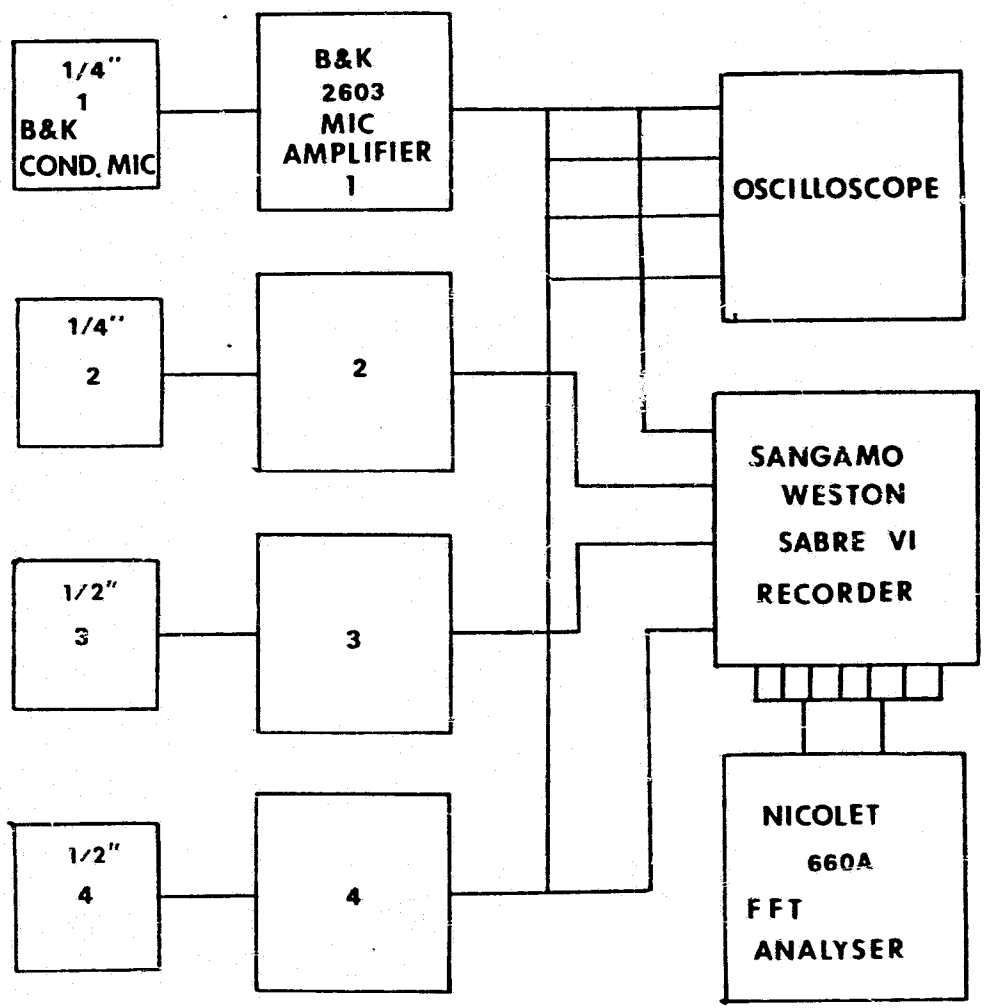

FIGURE 5 : Instrumentation for Near Field Pressure Measurements

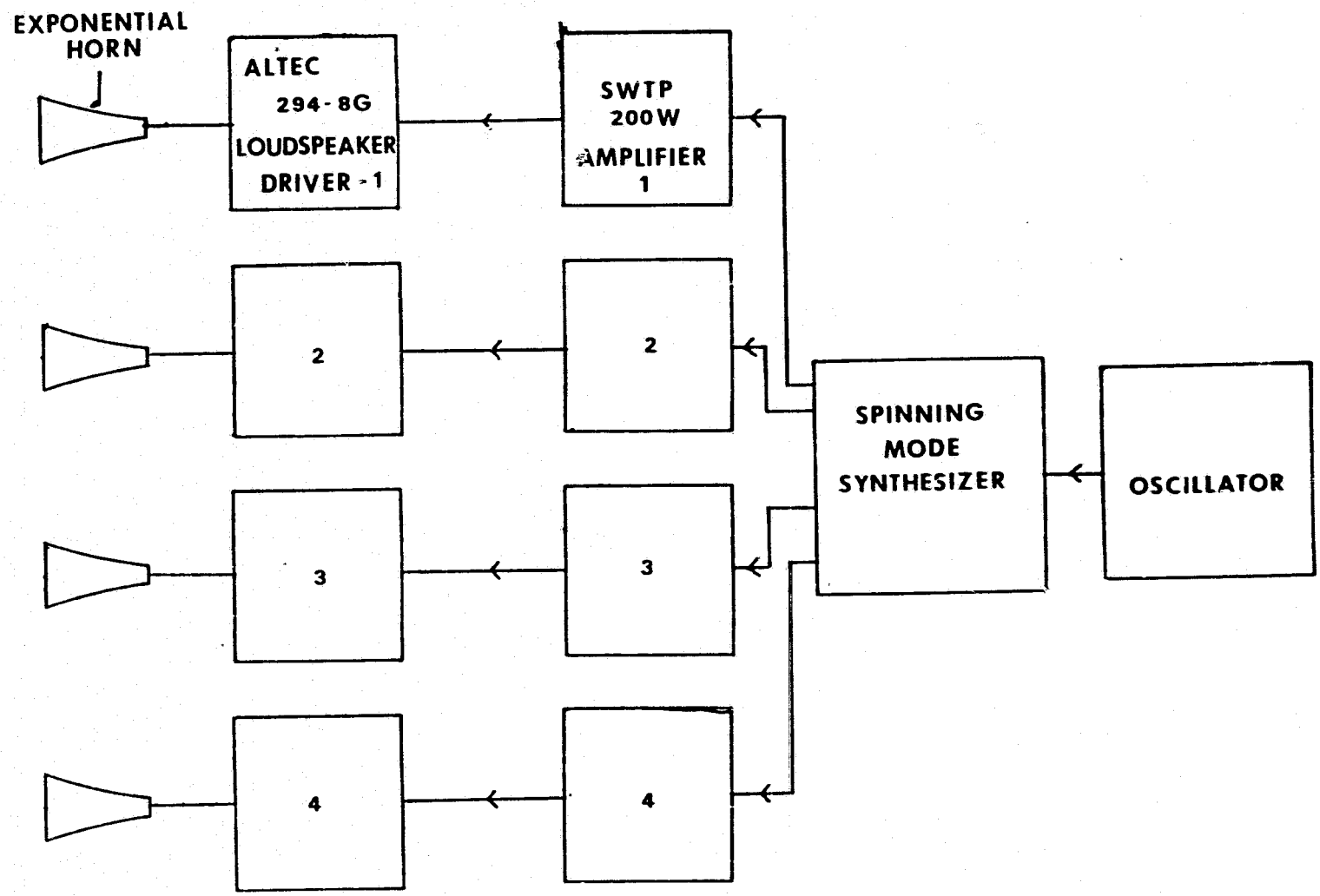

FIGURE 6 : Acoustic Excitation System

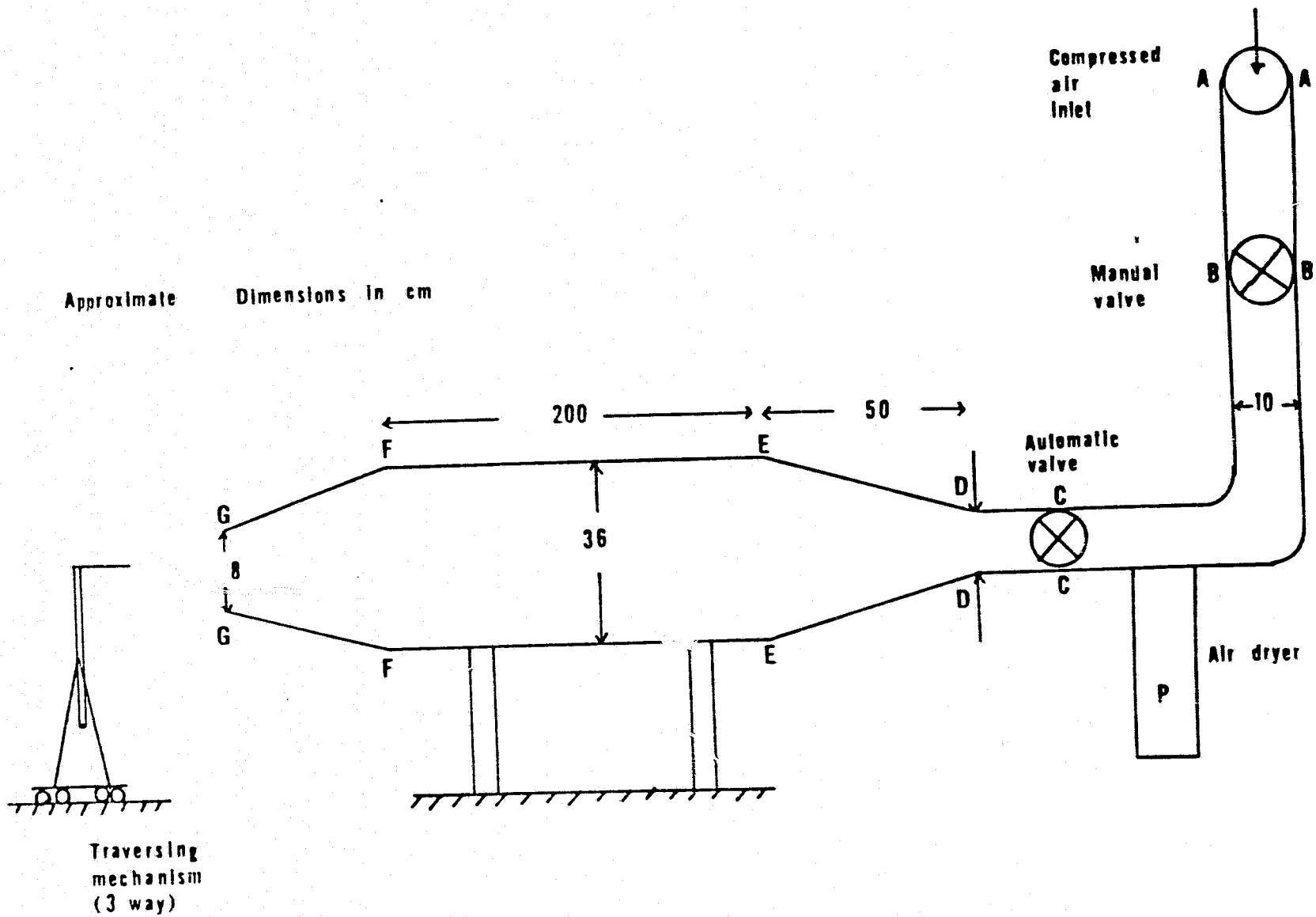

FIGURE-7- Proposed Jet Facility

AIAA-80-1004

A Model for Broadband Jet Noise Amplification

P. J. Morris, Pennsylvania State University, University Park, Pa.

AIAA 6th AEROACOUSTICS CONFERENCE

June 4-6, 1980/Hartford, Connecticut

A MODEL FOR BROADBAND JET NOISE AMPLIFICATION

Philip J. Morris *
Department of Aerospace Engineering
The Pennsylvania State University
University Park, Pennsylvania 16802

Abstract

A model is proposed for the change in turbulent structure of a round jet in the presence of an acoustic excitation. The excitation is assumed to trigger instability waves of a known initial amplitude at the jet exit. As these waves propagate downstream they extract energy from the mean flow and transfer it to the random turbulence. This results in an increase in the levels of the turbulence and a resulting increase in the radiated broadband noise. No calculations are presented for the noise radiation, however, an examination is made of the effect of excitation level and frequency on the jet flow. The numerical procedure allows for radial as well as axial variations in the averaged properties of jet to be calculated. The results indicate that the presence of a finite amplitude instability wave increases the spreading of the jet. It does not vary the characteristic radial shapes of both the axial mean velocity and the turbulent kinetic energy. An energy budget for the fandom turbulence shows that it is fed energy from the excited wave predominantly on each side of the jet lip line. This results in a broader radial shape for the turbulent kinetic energy.

Introduction

It is now generally acknowledged that turbulent shear flows, particularly free shear flows, possess a large scale structure. However, the role that this structure plays in the generation of sound by turbulence and even the nature of these large scale motions such as their orderliness, particularly at high Reynolds numbers, remains an open question. It appears that at high subsonic and supersonic velocities in jets and mixing layers the large scale motion may be associated with wavelike instabilities of the primary flow. Since the phase velocity of these travelling waves is of the order of the speed of sound in the surrounding medium the instability waves radiate sound, of a highly directional nature, very efficiently. Calculations by Tam and Morris[1] and Morris and Tam[2] show that successful predictions of radiated noise from supersonic jets and mixing layers, at angles in the far field that include the peak polar noise angle, may be made assuming that the radiation comes from instability waves. When the characteristic mean velocity is subsonic the role of the large scale structure in noise radiation is less clear. At these velocities the phase velocity of instability waves, if such waves are a reasonable model of the large structure, is much less than the ambient speed of sound, so that even allowing for spatial variations in the wave amplitude and phase velocity (see refs. 1 and 2) these waves are very inefficient radiators of sound. It appears more likely that it is the degree of disorderliness of the large structures and the fine scale turbulence which controls subsonic noise radiation.

However at subsonic, and most likely supersonic, flow velocities the large scale structure can effect noise radiation, in an indirect way. If large scale motions are excited in the jet by, for example, acoustic excitation at the jet exit then the sound radiation of the jet increases. Surprisingly, even if the excitation is at a single frequency the increase in noise radiation may occur at all frequencies. This phenomenon has been observed by Bechert and Pfizenmaier[3], Moore[4] and Schmidt[5]. Moore, Schmidt, and Vlasov and Ginevskiy[6] also observed that the levels of turbulence in these excited jets also changed. The variation in the turbulence levels and the radiated noise was found to be a function of excitation level, frequency and azimuthal mode number. At high excitation frequencies there was some reduction in the broadband noise radiation.

In this paper a model is presented for the mechanisms by which the structure of the turbulence is modified by a pure tone excitation. The basic formulation is similar to those used previously by this author and others, most closely to Chan[7] to study the characteristics of wave-like disturbances in turbulent jets. However this paper is concerned with the variation of the random component of the flow. The presence of a periodic component of finite amplitude is able to modify both the levels of the random turbulence and the mean flow characteristics. Previous analyses, because of the obvious simplification introduced, have made use of integral forms of the momentum and energy equations for the mean, periodic and random turbulent motion. Though this has permitted the axial variations in integral flow properties to be calculated radial variations are suppressed. For example the mean velocity profile is represented by a shape function which remains independent of the excitation level, etc. The present formulation permits the radial variations, if any, to be computed.

Though the analysis of this paper is more general than previous work there remain closure problems and, in the absence of the necessary guidance yet to be provided by experiments, some simple schemes have been adopted. Thus this paper also provides a framework within which improved closure models may be tested.

The model to be explored in the present paper argues that the acoustic excitation stimulates instability waves on the jet column. The amplitude of these waves will be determined, initially, by the level of the excitation. Tam[8,9] has developed an analysis to determine the amplitude of the excited waves in the linear region, where the amplitude of the excited wave is linearly propor-

* Assistant Professor, Member AIAA

tional to the amplitude of the excitation. The coupling that occurs between the acoustic excitation occurs over the entire region adjacent to the mixing layer (all along the potential core in the jet flow for internal excitation). However because of the mismatch in phase velocity between the instability and sound waves the coupling is greatest close to the jet exit. In the present analysis the full coupling procedure as proposed by Tam will not be used, rather the level of the instability wave at the jet exit will be assumed to be known. There is no reason why Tam's analysis could not be incorporated; however, because of the iterative nature of the present solution and the axial variation in the shape of the mean velocity profile it would be computationally time-consuming.

The presence of an instability wave of finite magnitude performs two roles. Firstly it extracts energy from the mean flow in the initial region of the jet though some is returned as the wave decays. Secondly it interacts with the random turbulence. This interaction involves both the generation of additional turbulent energy and its transport. The increase in the level of the random turbulent kinetic energy causes a more rapid spreading of the jet flow through an increase in turbulent stresses and, it can be argued, an increase in the broadband noise radiation. No details are provided in the present paper of the anticipated increase in the broadband noise radiation. The paper is more concerned with changes in the turbulent structure. If the noise producing volume of the jet is relatively unchanged by the presence of the excited waves then the increase in turbulence levels is likely, using scaling arguments, to yield increases in the radiated noise. Once the details of the modification to the flow are known the noise changes may be calculated. However, if no details of the flow changes are given then no estimate of the noise variation is possible.

Mathematical Derivation

Basic Equations

In the formulation of the present analysis several simplifying assumptions have been made; these are described at the appropriate point in the text. It is useful to start using generalized coordinates and then carry out the simplifications provided by the geometry and the physical nature of the problem at a later stage. The incompressible momentum and continuity equations in tensor form are

$$\frac{\partial u^i}{\partial t} + u^j u^i_{,j} = -\frac{1}{\rho}\frac{\partial p}{\partial x^j} g^{ij} + \nu g^{jk} u^i_{,jk} , \quad (1)$$

and

$$u^i_{,i} = 0 \quad (2)$$

where u^i is the contravariant velocity tensor, p is the pressure, g^{ij} is the metric tensor and the usual notation has been used for covariant differentiation. The instantaneous velocity and pressure are separated into three components

$$u^i = \bar{u}^i + \tilde{u}^i + u'^i , \quad (3a)$$

and

$$p = \bar{p} + \tilde{p} + p' \quad (3b)$$

where an overbar denotes a time-independent component, a prime denotes a random turbulent time-dependent component and a tilde denotes a periodic component which is related in phase to the acoustic excitation at the nozzle exit. The time average of a variable is defined as

$$\bar{f} = \lim_{T\to\infty} \frac{1}{T}\int_0^T f(t)dt , \quad (4)$$

and the phase average is defined by

$$\langle f \rangle = \lim_{N\to\infty} \frac{1}{N}\sum_{n=1}^{\infty} f(t + n\tau) \quad (5)$$

where τ is the period of the excitation. It is readily shown that all components of u^i satisfy the same continuity equation,

$$\bar{u}^i_{,i} = \tilde{u}^i_{,i} = u'^i_{,i} = 0 . \quad (6)$$

Taking the time average of equation 1 and using equation 6 gives,

$$\bar{u}^j \bar{u}^i_{,j} = -\frac{1}{\rho}\frac{\partial \bar{p}}{\partial x^j} g^{ij} - \overline{(\tilde{u}^j \tilde{u}^i)}_{,j} - \overline{(u'^j u'^i)}_{,j} , \quad (7)$$

where the Reynolds number is assumed sufficiently high for the viscous stresses to be neglected. The random disturbance momentum equation is obtained by taking the phase average of equation 1 from the full equation, giving,

$$\frac{\partial u'^i}{\partial t} + \bar{u}^j u'^i_{,j} + u'^j \bar{u}^i_{,j} = -\frac{1}{\rho} g^{ij}\frac{\partial p'}{\partial x^j} + \nu g^{jk} u'^i_{,jk} - \tilde{u}^j u'^i_{,j} - u'^j \tilde{u}^i_{,j} - (u'^j u'^i_{,j} - \langle u'^j u'^i_{,j}\rangle) \quad (8)$$

The equation for the turbulent kinetic energy is obtained by multiplying equation 8 by $g_{im}u'^m$ and averaging. After some manipulation the resulting equation is

$$\bar{u}^j k_{,j} = -\overline{u'^m u'^j}\,\bar{u}_{m,j} - \frac{1}{\rho}\overline{(u'^m p')}_{,m} - \overline{(u'^j k')}_{,j} - \bar{\tilde{r}}^j_i \bar{\tilde{u}}^i_{,j} - \overline{(\tilde{u}^j \tilde{r}^i_i)}_{,j} - \varepsilon \quad (9)$$

where $k' = 1/2\, u'^j u'_j$ is the fluctuating turbulent kinetic energy, $k = \overline{k'}$ and ε is the viscous dissipation term. $\tilde{r}^j_i$ is the "wave-induced stress" given by,

$$\rho\tilde{r}^j_i = g_{ik}\rho\{\langle u'^k u'^j\rangle - \overline{u'^k u'^j}\} \quad (10)$$

It represents the difference between the Reynolds stresses, $\rho u'^i u'^j$ in the presence of the periodic disturbance and without it, since performing a phase average provides the sum of a time independent component and a periodic component. The first term on the right hand side of equation 9 represents the production of turbulent kinetic energy from the mean flow, the second and third terms represent turbulent transport, the fourth term is the interaction between the random and periodic fields (this is not a transport term and will be shown to always represent a net gain in turbulent kinetic energy), the fifth term is the transport of turbulent kinetic

energy by the periodic field and the last term is the viscous dissipation.

The equation for the wave kinetic energy is obtained by taking the time average of equation 1 from its phase average, multiplying by $g_{ik}\tilde{u}^k$ and time averaging. The resulting equation is,

$$\bar{u}^j \frac{\partial q}{\partial x^j} = -\overline{\tilde{u}^j\tilde{u}^k}\bar{u}_{k,j} - \frac{1}{\rho}\overline{(\tilde{p}\tilde{u}^k)}_{,k} - \overline{(\tilde{u}^j\tilde{q})}_{,j} + \overline{\tilde{r}_i^j\tilde{u}^i}_{,j} - \overline{(\tilde{u}^i\tilde{r}_i^j)}_{,j} \tag{11}$$

where $\tilde{q} = \frac{1}{2}\tilde{u}^j\tilde{u}_j$ is the wave kinetic energy, $q = \bar{\tilde{q}}$, and the viscous terms have been neglected.

Equations 6, 7, 9 and 11 provide the framework for the present analysis. In the next section the geometric simplifications and the turbulence closure schemes are introduced.

Turbulence Models

Cylindrical polar coordinates are used with the origin at the center of the circular jet nozzle and the z axis aligned with the jet centerline. The physical components of the contravariant tensor u^i are v, w/r, and u with respect to the r, ϕ and z coordinates. After several simplifications based on the assumptions that the time-averaged flow is axisymmetric and axial variations of time-averaged values are negligible with respect to radial variations the following system of equations is obtained.

$$\bar{u}\frac{\partial\bar{u}}{\partial z} + \bar{v}\frac{\partial\bar{u}}{\partial r} = -\frac{1}{r}\frac{\partial\overline{u'v'}r}{\partial r} - \frac{1}{r}\frac{\partial\overline{\tilde{u}\tilde{v}}r}{\partial r} , \tag{12}$$

$$\bar{u}\frac{\partial k}{\partial z} + \bar{v}\frac{\partial k}{\partial r} = -\frac{1}{r}\frac{\partial}{\partial r}\overline{v'(p' + k')}r - \overline{u'v'}\frac{\partial\bar{u}}{\partial r} - \varepsilon - \phi - \frac{1}{r}\frac{\partial\overline{\tilde{v}\tilde{r}_i^i}r}{\partial r} , \tag{13a}$$

where

$$\phi = \overline{\tilde{r}_i^j\tilde{u}^i}_{,j} . \tag{13b}$$

The integral form of equation 11 which will be used in the subsequent analysis is given by

$$\frac{d}{dz}\int_o^\infty \bar{u}qrdr = -\int_o^\infty \overline{\tilde{u}\tilde{v}}\frac{\partial\bar{u}}{\partial r}rdr + \int_o^\infty \phi\, rdr . \tag{14}$$

In the above equations the velocities have been non-dimensionalized with respect to the average jet exit velocity $\bar{u}_J$, lengths with respect to the jet radius r_J, and the pressure with respect to $\rho_J u_J^2$ where ρ_J is the jet exit density (equal to the density everywhere in the present formulation).

Examination of the equations above indicate that several turbulence models are required. In equation 12 both the random Reynolds stresses and the averaged wave stresses must be modelled. In equation 13a the turbulent diffusion, viscous dissipation, wave induced stresses and "wave transport" must be modelled. In the present analysis it is the modelling of the latter two effects which are of most interest thus a conventional "one-equation model" will be used to describe the random Reynolds stresses. Following Chan[7], set

$$-\overline{u'v'} = \varepsilon_t\frac{\partial\bar{u}}{\partial r} \tag{15a}$$

with

$$\varepsilon_t = C_1 k^{1/2}\ell , \tag{15b}$$

where ℓ is taken as the width of the jet mixing layer between radii at which $\bar{u} = 0.9$ and 0.1 respectively. A gradient transport hypothesis is used for the turbulent diffusion,

$$-\overline{v'(p' + k')} = \frac{\varepsilon_t}{\sigma_k}\frac{\partial k}{\partial r} , \tag{16}$$

and dimensional arguments provide the energy dissipation rate as

$$\varepsilon = C_2\frac{k^{3/2}}{\ell} \tag{17}$$

The coefficients C_1, C_2 and σ_k take the values 0.05, 1.50 and 0.7 respectively. These models would enable the jet development to be calculated in the absence of an excitation. Now consider the "wave-induced stresses." By analogy with the Reynolds stress model they could be written

$$\tilde{r}_i^j = -2\,\tilde{\varepsilon}_t\tilde{s}_i^j , \tag{18}$$

where $\tilde{s}_i^j$ is the periodic rate of strain tensor,

$$\tilde{s}_i^j = \frac{1}{2}(u^j_{,i} + g^{jk}u_{i,k}) . \tag{19}$$

The choice of $\tilde{\varepsilon}_t$ will be discussed below. Contraction of equation 18 leads to

$$\tilde{r}_i^i = 2(\langle k'\rangle - k) = -2\,\tilde{\varepsilon}_t\tilde{s}_i^i . \tag{20}$$

However from the continuity equation, $\tilde{s}_i^i = 0$, so that the random kinetic energy in the presence of an excitation is equal to its value without excitation, which is in disagreement with observations. Thus equation 18 should be written,

$$\tilde{r}_i^j = -2\,\tilde{\varepsilon}_t\tilde{s}_i^j + \frac{2}{3}(\langle k'\rangle - k)\delta_i^j . \tag{21}$$

Now consider the choice of $\tilde{\varepsilon}_t$. The value of ε_t is given by equation 15b as $C_1 k^{1/2}\ell$. This is a consequence of the assumption that there is only one characteristic time scale for the random and mean flows (see Tennekes and Lumley[10]). Letting this time scale be $\bar{t}$ the eddy viscosity may be written

$$\varepsilon_t = C_3 k\bar{t} \tag{22}$$

If the time scale for the periodic field is denoted by $\tilde{t}$ the periodic eddy viscosity could be written as

$$\tilde{\varepsilon}_t = C_4 k\tilde{t} , \tag{23a}$$

or

$$C_5\varepsilon_t/\tilde{\varepsilon}_t = \bar{t}/\tilde{t} , \tag{23b}$$

where C_3, C_4 and C_5 are unknown coefficients. Now $u_J\tilde{t}/r_J = 2\pi/\omega = 1/f$, where ω and f are the non-dimensional radian frequency and frequency of the periodic excitation, respectively, and $\bar{t} = \ell/k^{1/2}$. So that

$$\frac{\tilde{\ell}}{\tilde{t}} = k^{1/2} \cdot \frac{St}{2\ell} , \qquad (24)$$

where the Strouhal number, $St = f^* d_j / u_j$, where f^* is the dimensional excitation frequency and d_j is the jet diameter. Thus,

$$\tilde{\varepsilon}_t = \frac{C_5 k}{2\,St} . \qquad (25)$$

Since the value of k varies little with axial distance the periodic eddy viscosity is nearly constant for any given frequency, and decreases with increasing frequency.

In the present paper the "wave-induced stresses" are modelled using equation 21. However the "wave transport" term in equation 13a is neglected. This term would have been zero if the model equation 18 had been used. This means that a further model for the quantity $\tilde{v}\langle k' \rangle$ is not required. It should be noted that Chan[7] used equation 18 with the resulting neglect of wave transport. However in his analysis, since he did not distinguish between source and transport terms, the wave interaction terms in his analysis contain many terms which would be eliminated using the continuity equation. In the present paper calculations have been performed assuming that $\tilde{\varepsilon}_t = \varepsilon_t$.

From equations 13b, 18, and 19 an expression for ϕ may be obtained. In the present paper only axisymmetric periodic disturbances have been considered. In this case ϕ simplifies to,

$$\phi_o = -\tilde{\varepsilon}_t \left\{ \overline{\left(\frac{\partial \tilde{u}}{\partial r} + \frac{\partial \tilde{v}}{\partial z}\right)^2} + \overline{\left(\frac{\partial \tilde{u}}{\partial z} - \frac{\partial \tilde{v}}{\partial r}\right)^2} + \overline{\frac{3\tilde{v}^2}{r^2}} \right\} \qquad (26)$$

Note that ϕ_o is always less than zero so that it represents a gain of turbulent kinetic energy and a loss of wave kinetic energy.

In light of the dynamic instability of the jet mean velocity profile it is reasonable to model the periodic flow field as large scale instability waves stimulated by the excitation at the jet exit. These will be modelled as linear waves whose wavelength and growth rates are the eigenvalue of a local inviscid stability calculation. So that a periodic disturbance is written, for example as,

$$\tilde{u} = A(z)\,\mathrm{Re}\{\hat{u}(r)\, \exp[i(\alpha z - \omega t)]\} , \qquad (27)$$

where α is the axial wavenumber and A(z) represents an axial amplitude variation. This can lead to some difficulties, particularly when the wave is decaying. In such cases the inviscid solution is not valid over the entire real radial axis. (Physically correct damped inviscid solutions do exist. However they require a contour deformation into the complex r-plane; see Tam and Morris[1].) In order to overcome this difficulty the instability wave characteristics will be obtained from a local viscous stability calculation. The Reynolds number used in the calculations is sufficiently high that the solutions approach the inviscid limit. Following Tam and Chen[11] the value was chosen to be 500. Since it is the intent of this and subsequent analyses to consider both incompressible and compressible flows (to examine amplification effects in high Mach number jets) a technique has been developed to consider the stability of viscous, compressible axisymmetric jets. Though only results for axisymmetric disturbances in the incompressible limit are given in the main body of the paper, the complete analysis is given in Appendix A.

The stability analysis gives all the unknown quantities in equation 27 with the exception of the amplitude, A(z). This is obtained from equation 14 which now represents an ordinary differential equation for A(z).

$$\frac{1}{|A|^2}\frac{d}{dz}\left(|A|^2 I_1\right) = -I_2 - I_3 \qquad (28)$$

where

$$I_1 = \frac{1}{2}\int_o^\infty \bar{u}\left(|\hat{u}|^2 + |\hat{v}|^2\right) r\,dr , \qquad (29a)$$

$$I_2 = \frac{1}{2}\int_o^\infty \mathrm{Re}\{\hat{u}\hat{v}^*\}\frac{\partial \bar{u}}{\partial r}\, r\,dr , \quad \text{and} \qquad (29b)$$

$$I_3 = -\int_o^\infty \tilde{\varepsilon}_t \left\{ \left|\frac{\partial \hat{u}}{\partial r} + i\alpha\hat{v}\right|^2 + \left|i\alpha\hat{u} - \frac{\partial \hat{v}}{\partial r}\right|^2 + \frac{3|\hat{v}|^2}{r^2} \right\} r\,dr , \qquad (29c)$$

where an asterisk denotes the complex conjugate. In order to provide a consistent definition of A(z) the eigensolutions $\hat{u}$, $\hat{v}$ and $\hat{p}$ are normalized such that

$$|\hat{p}|^2 = 1 \quad \text{at} \quad r = 0 . \qquad (30)$$

Numerical Solution

The solution of equations 12, 13a and 28 has been obtained numerically using a technique which employs a standard three-point, variable step-size finite difference formulation in the radial direction with the axial derivative discretized in a manner which can either be fully implicit or explicit. It is hoped that sufficient details of the numerical scheme are provided below to enable the reader to use the technique. (It has been this author's experience that the distance between a numerical scheme and a working program is a very long one.)

Introducing the turbulence models given in the last section the axial momentum and turbulent kinetic energy equations may be written,

$$\bar{u}\frac{\partial \bar{u}}{\partial z} + \bar{v}\frac{\partial \bar{u}}{\partial r} = \frac{1}{r}\frac{\partial}{\partial r}\left[\varepsilon_t\, r \frac{\partial \bar{u}}{\partial r}\right] - \frac{1}{r}\frac{\partial \overline{\tilde{u}\tilde{v}} r}{\partial r} , \qquad (31)$$

and

$$\bar{u}\frac{\partial k}{\partial z} + \bar{v}\frac{\partial k}{\partial r} = \frac{1}{r}\frac{\partial}{\partial r}\left[\frac{\varepsilon_t}{\sigma_k}\, r \frac{\partial k}{\partial r}\right] + \varepsilon_t\left(\frac{\partial \bar{u}}{\partial r}\right)^2 - \frac{C_2 k^{3/2}}{\ell} - \phi_o . \qquad (32)$$

Drawing on the work of Spalding and Patankar[12] and Chan[7] new coordinates (ζ,ω) are introduced such that

$$\zeta = \frac{z}{4} \quad \text{and} \quad \omega = \frac{1}{\eta_e}\left[\int_o^r \bar{u}(z,s)\,s\,ds\right]^{1/2} . \qquad (33)$$

η_e^2 is a measure of the total axial volume flux in the jet. Due to entrainment this increases with axial distance and must be computed at each axial

location. The calculation of $d(\eta_e^2)/dz$ is described below. In terms of these new coordinates equations 31 and 32 become,

$$\frac{\partial \bar{u}}{\partial \zeta} = \frac{2\omega}{\eta_e^2}\frac{d(\eta_e^2)}{dz}\frac{\partial \bar{u}}{\partial \omega} + \frac{1}{\omega}\frac{\partial}{\partial \omega}\left\{\frac{r^2}{\omega}\varepsilon_t\frac{\bar{u}}{\eta_e^4}\frac{\partial \bar{u}}{\partial \omega}\right\} - \frac{2}{\eta_e^2}\frac{\partial}{\partial \omega}(\overline{\tilde{u}\tilde{v}}r) \quad , \tag{34}$$

$$\frac{\partial k}{\partial \zeta} = \frac{2\omega}{\eta_e^2}\frac{d(\eta_e^2)}{dz}\frac{\partial k}{\partial \omega} + \frac{1}{\omega}\frac{\partial}{\partial \omega}\left\{\frac{r^2}{\omega}\frac{\varepsilon_t}{\sigma_k}\frac{\bar{u}}{\eta_e^4}\frac{\partial k}{\partial \omega}\right\} + \frac{r^2}{\omega^2}\varepsilon_t\frac{\bar{u}}{\eta_e^4}\left(\frac{\partial \bar{u}}{\partial \omega}\right)^2 - \frac{4C_2 k^{3/2}}{\bar{u}\,\ell} - \frac{4\phi_o}{\bar{u}} \tag{35}$$

The flow field is divided into lines of constant ω denoted by the subscript i, $0 \le i \le N$, and lines of constant ζ denoted by the superscript j. Then at any point (i,j) the equations may be written,

$$\left(\frac{\partial \bar{u}}{\partial \zeta}\right)_i^j = \left\{a\frac{\partial^2 \bar{u}}{\partial \omega^2} + b\frac{\partial \bar{u}}{\partial \omega} + c\right\}_i^j \tag{36}$$

and,

$$\left(\frac{\partial k}{\partial \zeta}\right)_i^j = \left\{\frac{a}{\sigma_k}\frac{\partial^2 k}{\partial \omega^2} + d\frac{\partial k}{\partial \omega} + ek + f\right\}_i^j \tag{37}$$

The definitions of the functions a_i^j through f_i^j are given in Appendix B. The derivatives with respect to ω are written in a finite difference form such that

$$\left(\frac{\partial^2 s}{\partial \omega^2}\right)_i = \frac{2}{(1+\sigma)\sigma^{2i-1}(h_1)^2}\left(s_{i+1} - (1+\sigma)s_i + \sigma s_{i-1}\right) \tag{38a}$$

and

$$\left(\frac{\partial s}{\partial \omega}\right)_i = \frac{1}{(1+\sigma)\sigma^i h_1}\left(s_{i+1} + (\sigma^2 - 1)s_i - \sigma^2 s_{i-1}\right) \tag{38b}$$

where s is either $\bar{u}$ or k, h_i is the stepsize given by $(\omega_i - \omega_{i-1})$ and σ is the step-size ratio h_i/h_{i-1}, which is constant. Setting,

$$\left(\frac{\partial s}{\partial \zeta}\right)_i = g(s_{i-1}, s_i, s_{i+1}) = g_i \quad ,$$

the axial derivative is discretized in the usual finite-difference fashion,

$$s_i^{j+1} - s_i^j = (1-\lambda)\Delta\zeta g_i^j + \lambda\Delta\zeta g_i^{j+1} \quad , \tag{39}$$

where $\Delta\zeta$ is the axial step-size. If $\lambda = 0$ this is an explicit form, $\lambda = 1$ is an implicit form and $\lambda = 1/2$ is the Crank-Nicolson form. The last was used in the present calculations and was found to give rapid convergence. Substitution of these forms into equations 36 and 37 enables them to be written as either a pair of tridiagonal matrices or as a single 2 x 2 block tridiagonal matrix. The latter form, used in the present work is,

$$\underline{X}_i\,\underline{V}_{i-1}^{j+1} + \underline{Y}_i\,\underline{V}_i^{j+1} + \underline{Z}_i\,\underline{V}_{i+1}^{j+1} = \underline{d}_i \quad , \quad \text{for} \quad i = 1, N-1 \tag{40}$$

where the solution vector $\underline{V}_i = (\bar{u}_i, k_i)^T$, and the remaining matrices are given in Appendix B. The boundary conditions are that the axial velocity and turbulent kinetic energy are symmetric about r = 0 and they both vanish at large r. This leads to values of $\underline{X}_i$, $\underline{Y}_i$, $\underline{Z}_i$ and $\underline{d}_i$ for i = 0 and N which are also given in Appendix B.

Equation 40 and the additional equations provided by the boundary conditions may be solved by a standard algorithm for inversion of a block tridiagonal matrix. However the axial variation of (η_e^2) and the initial conditions must first be specified.

Calculation of $d(\eta_e^2)/dz$

At the outer edge of the jet $\partial\bar{u}/\partial\zeta \to 0$ and $\omega \to 1$. Thus from equation 34,

$$-\frac{d(\eta_e^2)}{dz} = \lim_{r\to\infty}\left\{\frac{\partial}{\partial r}(\varepsilon_t r) + \varepsilon_t r\frac{\partial^2 \bar{u}/\partial r^2}{\partial \bar{u}/\partial r} - \frac{\partial(\overline{\tilde{u}\tilde{v}}r)/\partial r}{\partial \bar{u}/\partial r}\right\} \tag{41}$$

Following Spalding and Patankar[12] the second term is ignored and the last term will be allowed for by writing,

$$-\frac{d(\eta_e^2)}{dz} = \lim_{r\to\infty}\left\{(1+\theta)\frac{\partial}{\partial r}(\varepsilon_t r)\right\} \tag{42}$$

The right hand side is approximated by its value at $\omega = \omega_{N-1}$. Then if,

$$G(\omega,z) = -(1+\theta)\varepsilon_t\left\{1 + \frac{r}{4}\frac{\bar{u}}{\eta_e^2}\frac{1}{k}\frac{\partial k}{\partial \omega}\right\} \tag{43}$$

Then,

$$\frac{d(\eta_e^2)}{dz} = (1-\lambda)G_{N-1}^j + \lambda\tilde{G}_{N-1}^{j+1} \tag{44}$$

and,

$$(\eta_e^2)^{j+1} = (\eta_e^2)^j + 4\Delta\zeta(1-\lambda)G_{N-1}^j + 4\Delta\zeta\lambda\tilde{G}_{N-1}^{j+1} \quad , \tag{45}$$

where the tilde denotes the estimate of G from a previous iteration.

The Initial Conditions

The mean velocity profile at the jet exit was taken to be the developed mixing layer form given by Maestrello and McDaid[13],

$$\bar{u}(r,0) = \begin{cases} \exp[-15.3825(r-0.796)^2] & r > 0.796 \\ 1.0 & r \le 0.796 \end{cases} \tag{46}$$

Choice of this developed profile for the shape at z = 0 does ignore the short region of adjustment at the jet exit from the boundary-layer-like profile of the jet nozzle. The initial value of ℓ is then 0.304. The turbulent kinetic energy profiles were estimated using a constant eddy viscosity assumption which leads to

$$k = 0.2277(r - 0.796)\bar{u} \quad , \quad r > 0.796 \quad (47)$$

In the potential core region the turbulent kinetic energy was set to a constant value of 6×10^{-4} which corresponds to a typical exit turbulence intensity of 2 percent.

These initial conditions though readily specified are somewhat idealized particularly in the potential core and result in a non-realistic behavior of the jet in the potential core region. From equation 35 it can be seen that if both k and $\bar{u}$ are constant the turbulence can only decay. This was observed in the calculation and resulted in an extension of the potential core length. However this paper is concerned with modification to a basic undisturbed flow by an acoustic excitation rather than absolute behavior thus no effort has been made to correct this behavior. Such a correction will be made in later calculations.

With $\bar{u}$ specified the variation of ω with r may be calculated from equation 33. The values of $\bar{u}$ at the grid values of ω were then determined using a cubic spline fit for $\bar{u}(\omega)$.

Calculation of r from ω and $\bar{u}(\omega)$

At each axial location the value of radial position must be calculated from the local values of ω and $\bar{u}$. Letting $f(\omega) = \omega/\bar{u}$ and using equation 33

$$(r^2)_i = (r^2)_{i-1} + 4\eta_e^2 h_i \int_0^1 f(t)dt \quad , \quad (48a)$$

where

$$t = (\omega - \omega_{i-1})/h_i \quad . \quad (48b)$$

A cubic polynomial spline fit may be obtained for f(t) on the interval (ω_{i-1}, ω_i) and finally,

$$(r^2)_i = (r^2)_{i-1} + 4\eta_e^2 h_i \left\{\frac{(f_i + f_{i-1})}{2} - \frac{h_i^2}{24}(K_i + K_{i-1})\right\} \quad (49)$$

where

$$f_i = \frac{\omega_i}{\bar{u}_i} \quad \text{and} \quad K_i = \left\{\frac{\partial^2}{\partial\omega^2}\left(\frac{\omega}{\bar{u}}\right)\right\}_i \quad . \quad (50)$$

The Computer Program

The numerical method was programmed in FORTRAN and run on an IBM 3033 processor. A simplified flow chart is shown in Figure 1. After initializing the values of $\bar{u}$ and k at the grid points the eigensolutions of the Orr-Sommerfeld equation are obtained for that velocity profile. This gives the distributions of the periodic flow field. The integrals in equation 29 may be calculated as well as the radial distributions of the source term ϕ and the periodic stress gradient $[\partial(\overline{\tilde{u}\tilde{v}}r)/\partial r]/r$. The wave amplitude at the next location is then computed from equation 28. Estimates of the coefficients of the matrices in equation 40 may now be made and the values of $\bar{u}_i^{j+1}$ and k_i^{j+1} calculated using the matrix solver. The wave shapes and integrals at the downstream location are then calculated from the Orr-Sommerfeld equation using the estimated downstream velocity profile. Revised estimates of the wave amplitude may also be made and new estimates of the values of the matrix elements in equation 40 are made. The procedure is repeated until the mean velocity profile at the downstream location is unchanged by further iterations. This requirement was met in the present calculations when the sum of the root mean square differences between the new and old estimates of $\bar{u}^{j+1}$ at all the grid points was less than 0.011. This was found to ensure three decimal places of accuracy at each grid point.

The numerical method ensures that alterations in the mean flow properties due to the presence of a finite amplitude periodic structure can be observed in both the axial and radial directions, and that the "shape" of the mean velocity and turbulent kinetic energy profiles may alter. The grid constants and coefficients used in the present calculations are shown in Table 1 where $\Delta\zeta^{j+1} = \sigma_z \Delta\zeta^j$.

Table 1 Constants used in computer program.

σ	λ	θ	$\Delta\zeta^0$	σ_z
0.90	0.5	0.2	0.0436	1.1

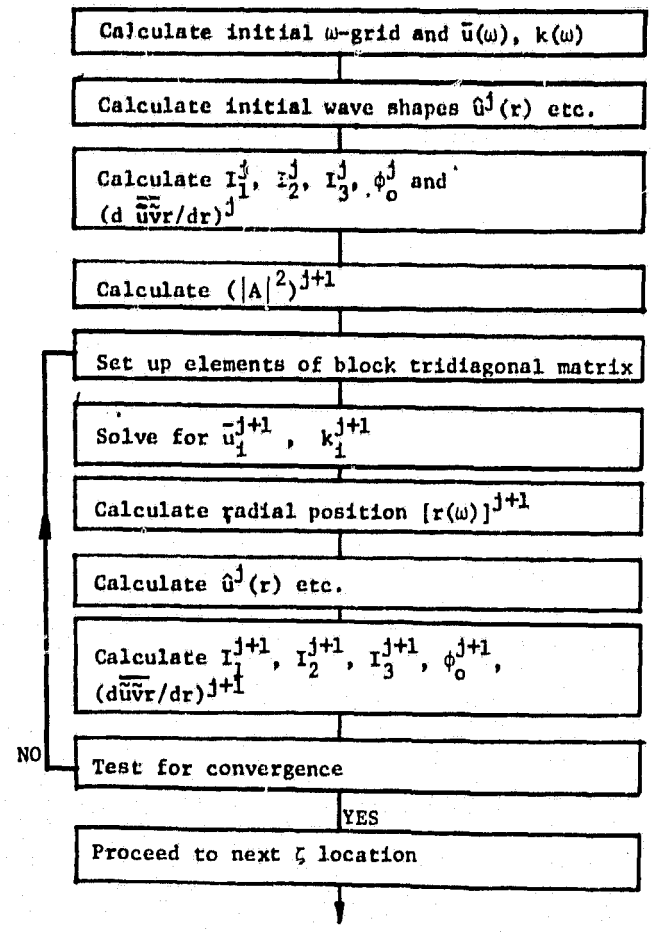

Fig. 1 Flow chart for computer program

Results and Discussion

Some preliminary calculations have been performed using the model described in the previous section. These calculations are viewed as an initial test of the method to provide guidance as to improved models.

The axial variation of the jet thickness for an unexcited jet is shown in Fig. 2. The variation approaches a linear increase with axial distance with a virtual origin of x = -2.0. This agrees with the measurements of Maestrello and McDaid[13] whose data were used as the initial velocity profile. A collapse of the computed mean velocity and turbulent kinetic energy profiles is obtained by using a stretched radial coordinate, $(r-1)/(x+2)$. These are shown in Figs. 3 and 4 respectively. Thus the unexcited jet behaves in agreement with experiment, though the spreading rate shown in Fig. 2 is somewhat low due to the idealized nature of the potential core mean velocity and turbulent kinetic energy profiles.

Most of the calculations have been performed for an excitation Strouhal number of 0.25. However in Fig. 5 the effect of Strouhal number of the jet spreading is shown. The spreading is greatest for St = 0.5 and least for St = 0.25. However the excitation level of $|A|_0^2 = 1 \times 10^{-4}$ was the minimum level at which modifications to the jet structure were observed. In all cases the jet spread rate increased. Fig. 6 shows the effect of increasing the excitation level by a factor of 10. The jet spreads initially more rapidly and then grows linearly for an excitation Strouhal number of 0.25.

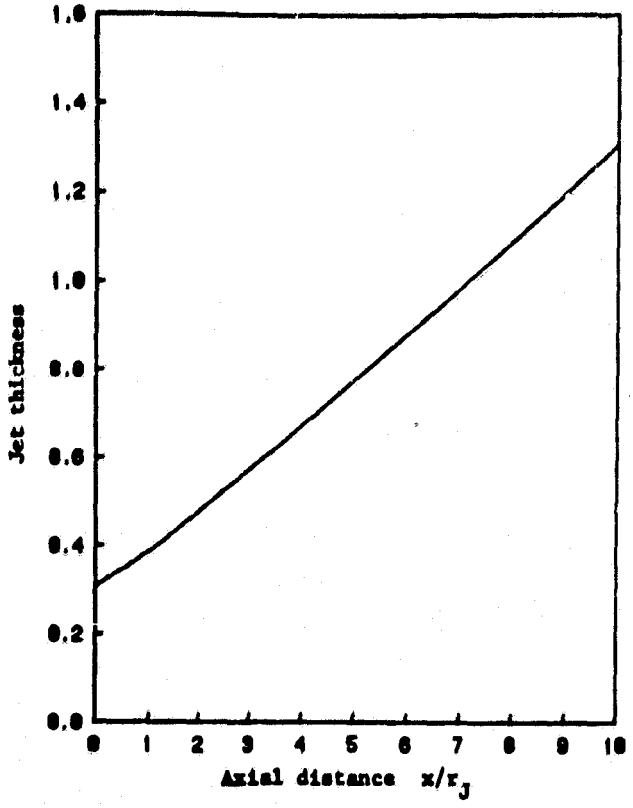

Fig. 2 Variation of jet thickness with axial distance

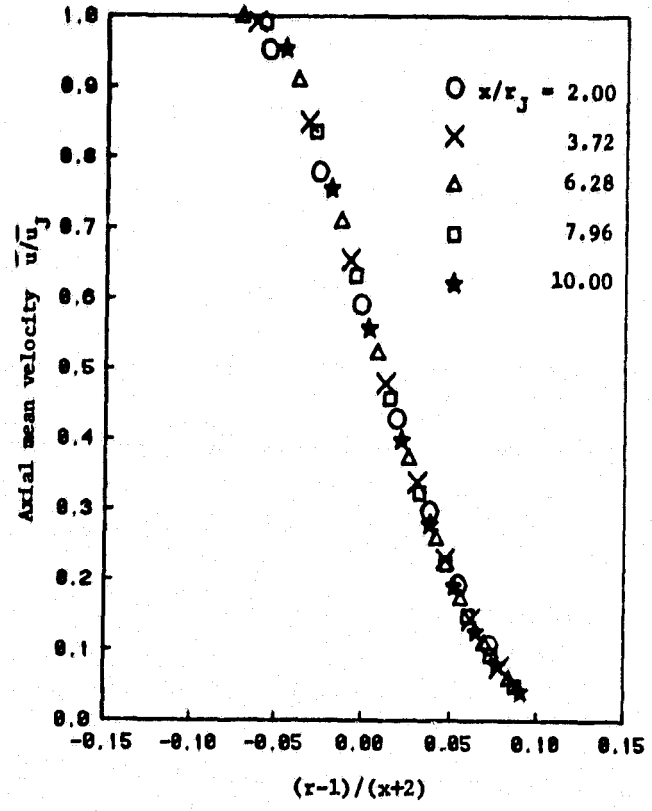

Fig. 3 Collapse of axial mean velocity with $(r-1)/(x+2)$

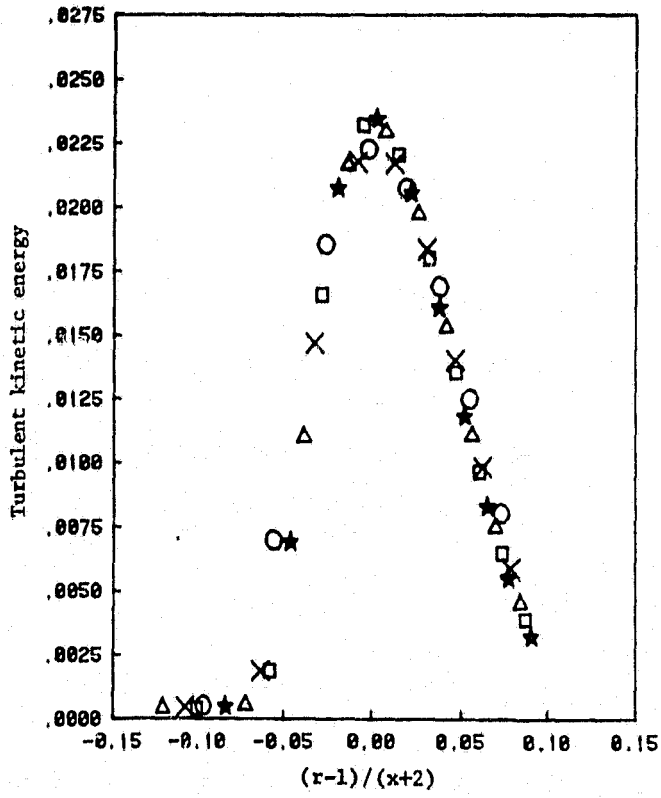

Fig. 4 Collapse of turbulent kinetic energy with $(r-1)/(x+2)$. For legend see Fig. 3

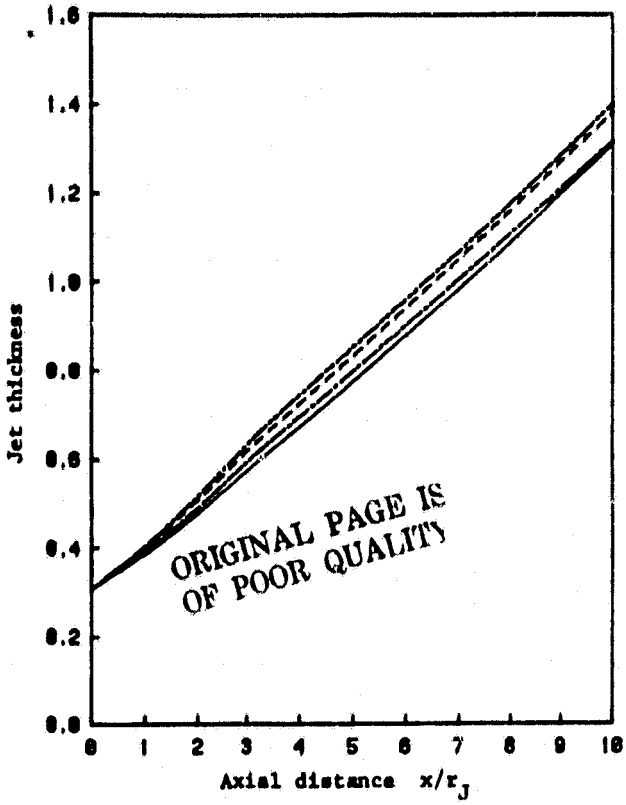

Fig. 5 Effect of excitation frequency on jet thickness. $|A|_o^2 = 1 \times 10^{-4}$. St = 0.1, ----; St = 0.25, – – – –; St = 0.50, – – – – –. No excitation ———.

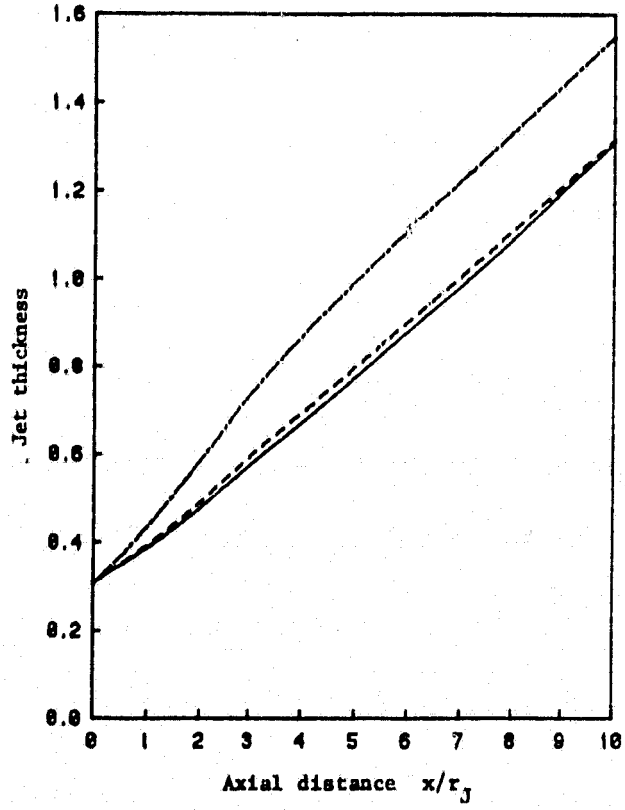

Fig. 6 Effect of excitation amplitude on jet thickness. St = 0.25. $|A|_o^2 = 1 \times 10^{-4}$, ----; $|A|_o^2 = 1 \times 10^{-3}$, – – – –. No excitation, ———.

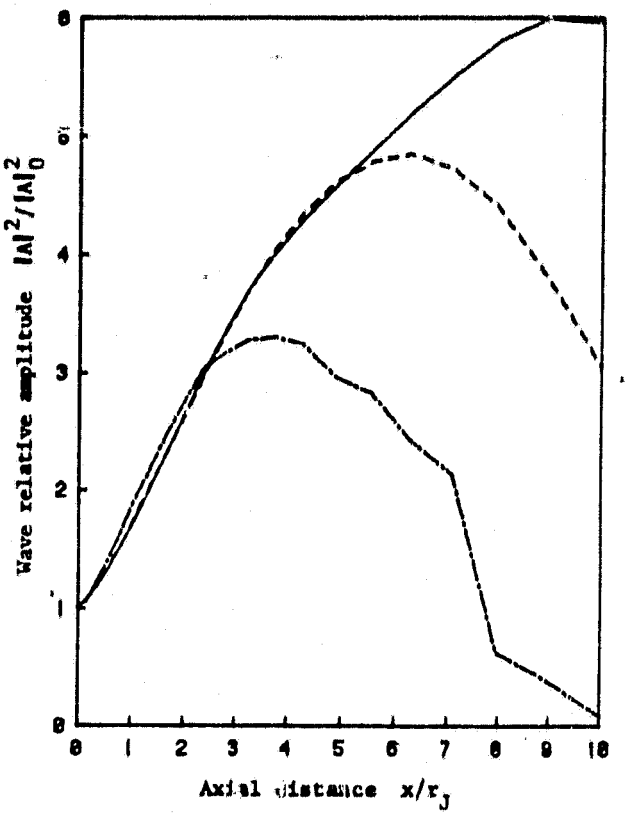

Fig. 7 Variation of relative amplitude of wave, $|A|^2/|A|_o^2$, with axial distance. St = 0.25. For legend see Fig. 6.

The new virtual origin of mixing is at x = -3.75. The absolute levels of excitation needed to produce these effects are discussed below.

When there is no interaction between the wave and the flow field the local rate of growth is that predicted by inviscid linear stability theory. However, when the wave is of sufficient amplitude to generate significant "wave-induced stresses" the wave loses energy to the random turbulence. This can be seen in Fig. 7 where the ratio of the wave amplitude to its initial amplitude is shown. From the definition giving $|A|^2$ using the normalization of equation 30 it can be associated with the mean square pressure fluctuation on the jet axis. As the wave amplitude increases its rate of growth falls below that of the linear prediction. For an initial amplitude of 1×10^{-3} for x/r_J greater than 4.0 the wave transfers more energy to the random turbulence than it gains from the mean flow and it begins to decay. There is also some decrease in the growth rate due to changes in the shape of the mean velocity profile and the jet width. However for $|A|_o^2 = 1 \times 10^{-3}$ linear stability predicts wave growth up to $x/r_J = 5.5$.

The amount and distribution of the energy transferred to the turbulence is seen by performing a radial energy budget. This is shown in Fig. 8 for the unexcited case, for a jet width of 0.447 which occurs at $x/r_J = 1.66$. Fig. 9 shows the energy budget in the excited case at a similar jet width, 0.446, which occurs closer to the jet exit, $x/r_J = 1.07$, in this case. The additional term in the turbulent kinetic energy equation which describes the wave interaction effect is seen to peak on each side of the jet lip line at $r/r_J = 0.8$ and 1.2. Its peak

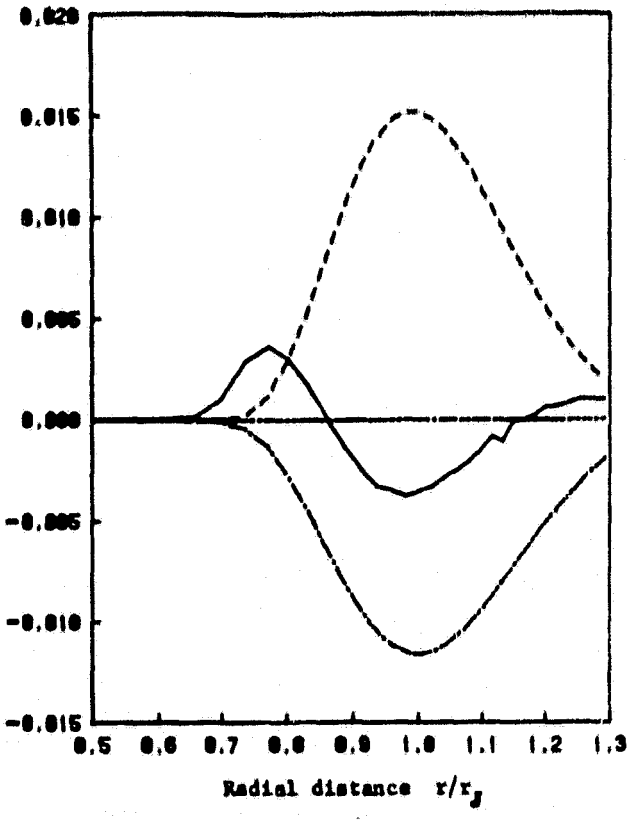

Fig. 8 Energy budget for no excitation. width = 0.447, x/r_J = 1.66. Production, ----; Diffusion, ——; Dissipation, ——·——; Wave interaction, ————.

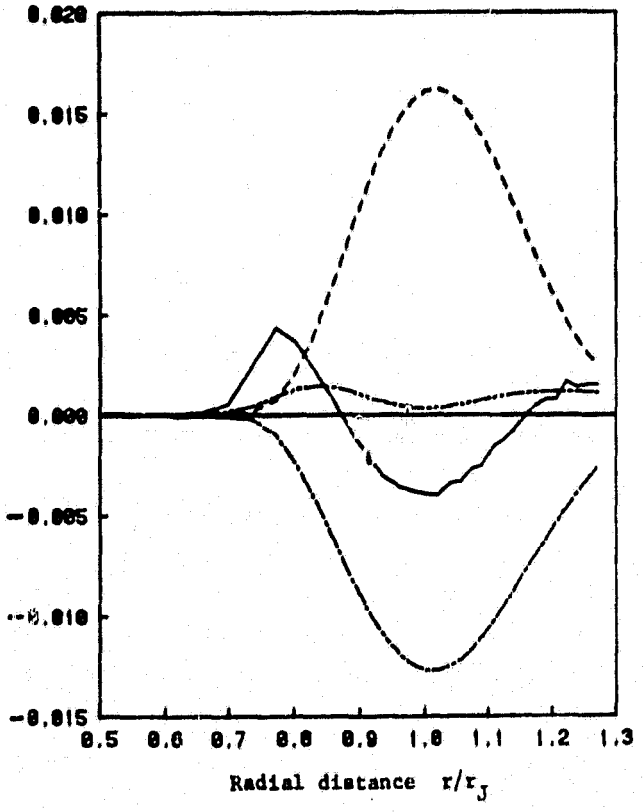

Fig. 9 Energy budget with excitation. St = 0.25, $|A|_o^2 = 1 \times 10^{-3}$, width = 0.446, x/r_J = 1.07. For legend see Fig. 8.

value is an order of magnitude less than the direct production from the mean flow, however since the other effects are almost in equilibrium, most of the production balanced by viscous dissipation, this has a significant effect.

The mean velocity profiles in the excited case are shown in Fig. 10. The shape of the wave profiles is such that in the potential core the wave transfers momentum to the mean flow. This results in a slight increase in the jet centerline velocity. The data all collapse using the same stretched coordinate, $(r-1)/(x+2)$, as used for the unexcited jet, with the exception of the profile at $x/r_J = 2.0$. However, this is to be anticipated since in this region the jet growth rate is more rapid. An initial look at the velocity shape, in comparison to Fig. 3 shows a broadening of the profile at the outer edge of the jet in agreement with the measurements of Schmidt.[5] However if a new virtual origin is chosen at $x/r_J = 3.75$ the calculations from both excited and unexcited jets are virtually identical. The same applies to the profiles of the turbulent kinetic energy which are shown in Fig. 11 as a function of $(r-1)/(x+3.75)$. The shape of the profile is unchanged from that of the unexcited jet except at the farthest downstream stations, $x/r_J = 7.96$ and 10.0. In these locations there is a rapid increase in the turbulent kinetic energy inside the lip line. At $x/r_J = 10.0$ there is a sudden increase in the peak level to 0.033 peaking at a radial location of $r/r_J = 0.66$. An initial look at the energy budget for this station indicates a sudden loss of energy by the wave which is also evidenced by its rapid decay shown in Fig. 7.

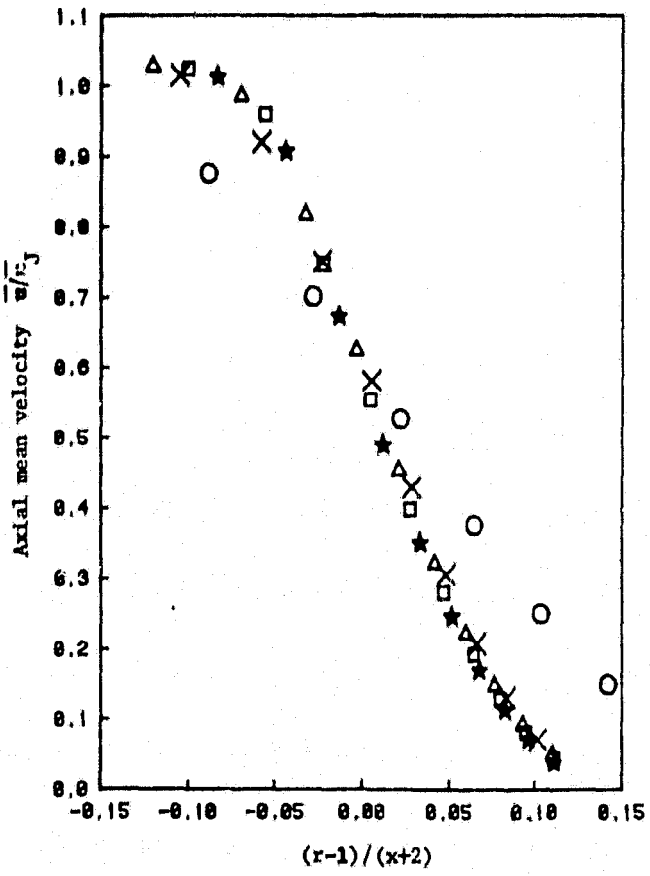

Fig. 10 Collapse of axial mean velocity with $(r-1)/(x+2)$ for excited jet. St = 0.25, $|A|_o^2 = 1 \times 10^{-3}$. For legend see Fig. 3.

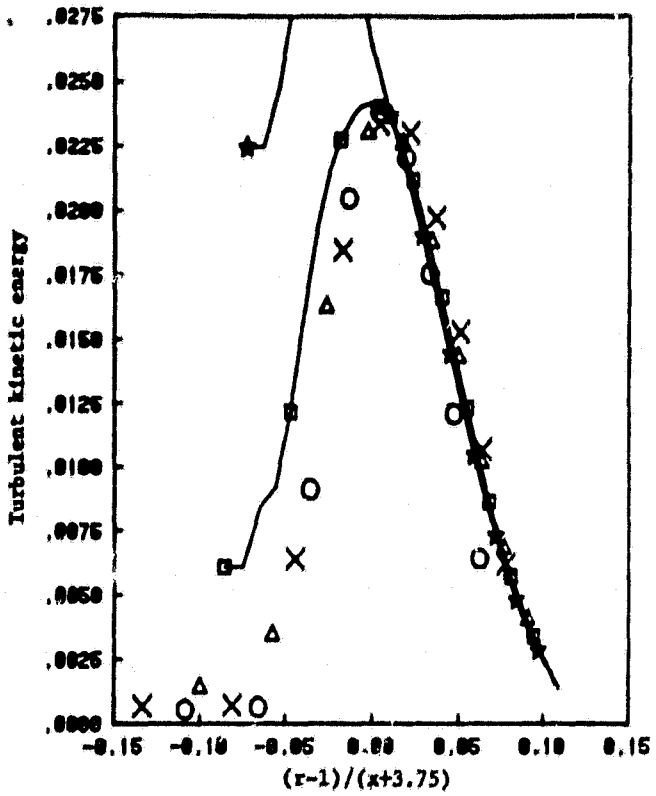

Fig. 11 Collapse of turbulent kinetic energy with $(r-1)/(x+3.75)$ for excited jet. St = 0.25, $|A|_o^2 = 1 \times 10^{-3}$. For legend see Fig. 3.

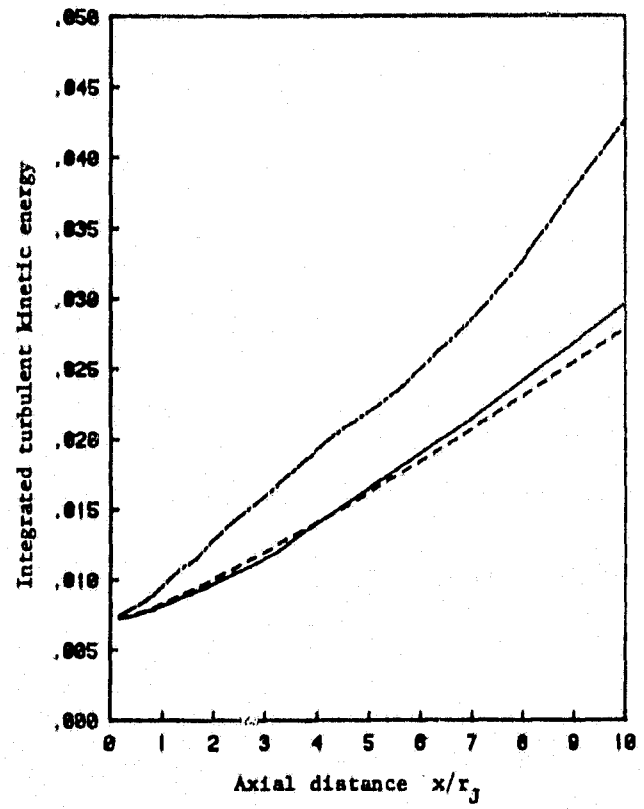

Fig. 12 Effect of excitation on radially integrated turbulent kinetic energy. For legend see Fig. 6.

The effect of excitation also increases the integrated turbulent kinetic energy given by,

$$\int_0^\infty k r dr \ .$$

This is shown in Fig. 12 where it can also be seen that at the lower excitation level there is a slight decrease in the integrated levels.

The choice of excitation level in these calculations has been determined by whatever value gave appreciable changes. As noted above the normalization used for the eigensolutions of the Orr-Sommerfeld equation means that $|A|_o^2$ is the mean square pressure fluctuation at the jet exit. Thus for $|A|_o^2$ of 1×10^{-4}, the lower excitation level, the pressure fluctuation at the jet exit is 2 percent of the dynamic head at the jet exit (taken as $\bar{\rho} u_j^2/2$). This is much larger than the minimum level observed by Moore of 0.08 percent. In order to achieve comparable effects with reduced excitation levels it would be necessary to increase the value of $\tilde{c}_t$.

Conclusions

The results indicate that the model can predict observed effects of acoustic excitation. However the absolute levels required do not match experiments. This may be attributed to the choice of model for the wave-induced stresses particularly its multiplicative constant. The results point to the need for a knowledge of the following:

1. further effects of frequency and excitation amplitude,
2. the effect of choice of coefficient in $\tilde{c}_t$,
3. the effect of permitting $\tilde{c}_t$ to be frequency dependent, and
4. the effect of inclusion of "wave-transport" terms in the turbulent kinetic energy equation.

There also exists a clear need for further experimental documentation of the changes in turbul ; structure. Without this guidance, development of appropriate models, for wave-induced stresses in particular, is made difficult.

Acknowledgments

The author acknowledges the support of NASA Langley Research Center under grant number 1580. The technical monitor is Dr. T. B. Gatski.

References

[1] Tam, C.K.W. and Morris, P.J., "The radiation of sound by the instability waves of a compressible plane turbulent shear layer," Journal of Fluid Mechanics, Vol. 98, Part 2, 1980, pp. 349-381.

[2] Morris, P.J. and Tam, C.K.W., "On the radiation of sound by the instability waves of a compressible axisymmetric jet," IUTAM/ICA/AIAA Symposium on the Mechanics of Sound Generation in Flows, Gottingen, Germany, August 28-31, 1979, Springer-Verlag, 1979, pp. 55-61.

[3] Bechert, D. and Pfizenmaier, E., "On the amplification of broadband jet noise by a pure tone excitation," AIAA Paper 76-489, July 1976.

[4] Moore, C.J., "The role of shear-layer instability waves in jet exhaust noise," Journal of Fluid Mechanics, Vol. 80, Part 2, 1977, pp. 321-367.

[5] Schmidt, C., "Aerodynamic characterization of excited jets," Journal of Sound and Vibration, Vol. 61, Part 1, 1978, pp. 148-152.

[6] Vlasov, Ye.U. and Ginevskiy, A.S., "Generation and suppression of turbulence in an axisymmetric turbulent jet in the presence of an acoustic excitation," NASA TTF 15721, 1974.

[7] Chan, Y.Y., "Nonlinear spatial wave development in an axisymmetrical turbulent jet," NRC Aero. Report LR-585, National Aero. Est. Ottawa, April 1975.

[8] Tam, C.K.W., "Excitation of instability waves in a two-dimensional shear layer by sound," Journal of Fluid Mechanics, Vol. 89, Part 2, 1978, pp. 357-371.

[9] Tam, C.K.W., "The effects of upstream tones on the large scale instability waves and noise of jets," IUTAM/ICA/AIAA Symposium on the Mechanics of Sound Generation in Flows, Gottingen, Germany, August 28-31, 1979, Springer-Verlag, 1979, pp. 41-47.

[10] Tennekes, H. and Lumley, J.L., A First Course in Turbulence, MIT Press, 1972.

[11] Tam, C.K.W. and Chen, K.C., "A statistical model of turbulence in two-dimensional mixing layers," Journal of Fluid Mechanics, Vol. 92, Part 2, 1979, pp. 303-326.

[12] Spalding, D.B. and Patankar, S.V., Heat and Mass Transfer in Boundary Layers, 2nd Ed., Int. Textbook Co., Ltd., London, 1970.

[13] Maestrello, L. and McDaid, E., "Acoustic characteristics of a high subsonic jet," AIAA Journal, Vol. 9, No. 6, June 1971, pp. 1058-1066.

[14] Dunn, D.W. and Lin, C.C., "On the stability of the laminar boundary layer in a compressible fluid," Journal of the Aeronautical Sciences, Vol. 22, 1955, pp. 455-477.

[15] Morris, P.J., "The spatial viscous instability of axisymmetric jets," Journal of Fluid Mechanics, Vol. 77, Part 3, 1976, pp. 511-529.

[16] Michalke, A., "Instabilität eines kompressiblen runden Freistrahls unter Berücksichtigung des Einflusses der Strahlgrenzschichtdicke," Z. Flugwiss., Vol. 19, 1971, pp. 319-328.

[17] Batchelor, G.K. and Gill, A.E., "Analysis of the stability of axisymmetric jets," Journal of Fluid Mechanics, Vol. 14, 1962, pp. 529-551.

Appendix A

Solution of the Viscous, Compressible, Linearized Stability Equations for an Axisymmetric Jet

In the analysis it is assumed, following Dunn and Lin[14] that the viscous dissipation terms in the energy equation may be neglected. Assuming that the mean velocity and density are functions of radius only the non-dimensional equations of motion may be written,

$$\frac{\partial \rho'}{\partial t} + \bar{\rho}\left(\frac{1}{r}\frac{\partial v' r}{\partial r} + \frac{1}{r}\frac{\partial w'}{\partial \phi} + \frac{\partial u'}{\partial z}\right) + v'\frac{d\bar{\rho}}{dr} + \bar{u}\frac{\partial \rho'}{\partial z} = 0 , \tag{A.1}$$

$$\bar{\rho}\left(\frac{\partial v'}{\partial t} + \bar{u}\frac{\partial v'}{\partial z}\right) + \frac{\partial p'}{\partial r} = \frac{1}{R}\left(\nabla^2 v' - \frac{v'}{r^2} - \frac{2}{r^2}\frac{\partial w'}{\partial \phi}\right) , \tag{A.2}$$

$$\bar{\rho}\left(\frac{\partial w'}{\partial t} + \bar{u}\frac{\partial w'}{\partial z}\right) + \frac{1}{r}\frac{\partial p'}{\partial \phi} = \frac{1}{R}\left(\nabla^2 w' - \frac{w'}{r^2} + \frac{2}{r^2}\frac{\partial v'}{\partial \phi}\right) , \tag{A.3}$$

$$\bar{\rho}\left(\frac{\partial u'}{\partial t} + \bar{u}\frac{\partial u'}{\partial z}\right) + \bar{\rho}\, v'\frac{d\bar{u}}{dr} + \frac{\partial p'}{\partial z} = \frac{1}{R}\nabla^2 u' , \tag{A.4}$$

where the velocity fluctuations in the r, ϕ and z directions are v', w' and u', respectively, and,

$$R = \frac{\rho_J u_J r_J}{\mu} \tag{A.5}$$

where ρ_J, u_J and r_J are the jet exit density, velocity and radius, respectively. Also

$$\nabla^2 \equiv \left\{\frac{\partial^2}{\partial r^2} + \frac{1}{r}\frac{\partial}{\partial r} + \frac{1}{r^2}\frac{\partial^2}{\partial \phi^2} + \frac{\partial^2}{\partial z^2}\right\} \tag{A.6}$$

Combining the energy and continuity equations leads to,

$$M_J^2\left\{\frac{\partial p'}{\partial t} + \bar{u}\frac{\partial p'}{\partial z}\right\} + \left\{\frac{\partial u'}{\partial z} + \frac{1}{r}\frac{\partial v' r}{\partial r} + \frac{1}{r}\frac{\partial w'}{\partial \phi}\right\} = 0 , \tag{A.7}$$

where $M_J^2 = u_J^2/a_J^2$ and a_J is the speed of sound at the jet exit. In equations (A.1) through (A.6) all variables have been non-dimensionalized with respect to the corresponding jet exit property and the pressure is non-dimensionalized by the dynamic head, $\rho_J u_J^2$, at the jet exit. Equations (A.2, 3, 4 and 6) provide four equations for the four unknown quantities, u', v', w' and p'.

The disturbances are written in a wave-like form so that a typical disturbance, q'(r,ϕ,z,t), may be written,

$$q'(r,\phi,z,t) = \mathrm{Re}\left\{\hat{q}(r)\exp[i(\alpha z - \omega t + m\phi)]\right\} \tag{A.8}$$

where α is the axial wavenumber, ω is the radian frequency and m is the azimuthal mode number. Substituting expressions of the form (A.8) into the equations of motion gives,

$$i\bar{\rho}(\alpha\bar{u} - \omega)\hat{v} + \hat{p}' = \frac{1}{R}\left\{\hat{v}'' + \frac{\hat{v}'}{r} - \left[\alpha^2 + \frac{(m^2+1)}{r^2}\right]\hat{v} - i\frac{2m}{r^2}\hat{w}\right\}, \tag{A.9}$$

$$i\bar{\rho}(\alpha\bar{u} - \omega)\hat{w} + \frac{im\hat{p}}{r} = \frac{1}{R}\left\{\hat{w}'' + \frac{\hat{w}'}{r} - \left[\alpha^2 + \frac{(m^2+1)}{r^2}\right]\hat{w} + i\frac{2m}{r^2}\hat{v}\right\}, \tag{A.10}$$

$$i\bar{\rho}(\alpha\bar{u} - \omega)\hat{u} + \bar{\rho}\bar{u}'\hat{v} + i\alpha\hat{p} = \frac{1}{R}\left\{\hat{u}'' + \frac{\hat{u}'}{r} - \left[\alpha^2 + \frac{m^2}{r^2}\right]\hat{u}\right\} , \tag{A.11}$$

and

$$iM_J^2(\alpha\bar{u} - \omega)\hat{p} + \left\{\hat{v}' + \frac{\hat{v}}{r} + \frac{im\hat{w}}{r} + \alpha\hat{u}\right\} = 0 \tag{A.12}$$

Primes denote differentiation with respect to r. For $M_J = 0$ and $\bar{\rho} = 1$ these equations reduce to the incompressible equations. For $\nu = 0$ or $R = \infty$ the equations reduce to their inviscid form. A solution for the former case for the axisymmetric jet was obtained by Morris[15] and for the inviscid case by Michalke[16]. The boundary conditions to be satisfied are[17]

$$\begin{aligned} &\hat{v}, \hat{w}, \hat{u}, \hat{p} \to 0 \quad \text{as} \quad r \to \infty \\ &\hat{u}(0) = \hat{p}(0) = 0 \qquad n \neq 0 , \\ &\hat{v}(0) = \hat{w}(0) = 0 \qquad n \neq 1 , \\ &\hat{v}(0) + i\hat{w}(0) = 0 \qquad n = 1 . \end{aligned} \tag{A.13}$$

As in the case of incompressible flow this sixth-order system of equations reduces into one fourth-order system and one second-order system for $m = 0$. That is, the $\hat{w}$ equation is not coupled to the equations for the remaining variables. Since the solution in this case, $m = 0$, is most readily obtained the analysis is described briefly below, and is then used to infer the general solution for arbitrary values of m.

In order to obtain a numerical solution to this problem it is necessary to determine the behavior of the solutions in the regions of uniform mean velocity, that is outside the jet flow and in the potential core region close to the jet axis. In the potential core region the non-dimensional mean velocity and density are unity. A series solution to the reduced equations is sought close to the jet axis. Thus the disturbances are written, making use of the boundary conditions for $m = 0$,

$$\begin{aligned} \hat{v} &= V_1 r + V_2 r^2 + V_3 r^3 + \cdots \\ \hat{u} &= U_o + U_1 r + U_2 r^2 + U_3 r^3 + \cdots \\ \hat{p} &= P_o + P_1 r + P_2 r^2 + P_3 r^3 + \cdots \end{aligned} \tag{A.14}$$

After some algebra it may be shown that,

$$\hat{p} = P_o\left\{1 + \frac{1}{4}\frac{[\alpha^2 R + i\lambda^2 M_J^2(\alpha - \omega)]}{[R_T + iM_J^2(\alpha - \omega)]} r^2 + \frac{1}{64}\frac{[\alpha^2 R + i\lambda^2 M_J^2(\alpha - \omega)]^2}{[R + iM_J^2(\alpha - \omega)]^2} r^4 + \cdots\right\} \tag{A.15}$$

where

$$\lambda^2 = \alpha^2 + i(\alpha - \omega)R . \tag{A.16}$$

This is the series expansion for the modified Bessel function of the first kind and zero order, that is,

$$\hat{p} = P_o I_o\left\{\sqrt{\frac{\alpha^2 R + i\lambda^2 M_J^2(\alpha - \omega)}{[R + iM_J^2(\alpha - \omega)]}} \cdot r\right\} \tag{A.17}$$

This expression reduces to the known solutions in the inviscid, and incompressible cases, that is, for

$$M_J = 0 \qquad \hat{p} = P_o I_o(\alpha r) , \tag{A.18}$$

and for

$$R \to \infty \qquad \hat{p} = P_o I_o\left(\sqrt{\alpha^2 - (\alpha - \omega)^2 M_J^2} \cdot r\right) \tag{A.19}$$

Inspection of the continuity equations then suggests the associated forms for $\hat{u}$ and $\hat{v}$ and substitution of these forms into the equations of motion yields,

$$\hat{u} = -P_o \frac{\alpha[R + iM_J^2(\alpha - \omega)]}{(\alpha - \omega)R} I_o(\lambda^* r) \tag{A.20}$$

$$\hat{v} = P_o \frac{i\lambda^*[R + iM_J^2(\alpha - \omega)]}{(\alpha - \omega)R} I_1(\lambda^* r) \tag{A.21}$$

where

$$\lambda^* = \sqrt{\frac{\alpha^2 R + i\lambda^2 M_J^2(\alpha - \omega)}{[R + iM_J^2(\alpha - \omega)]}} \tag{A.22}$$

It is clear that the disturbance pressure has only one linear solution which satisfies the boundary conditions. This is the so-called inviscid solution for incompressible viscous analyses. Since the momentum equations, which are the only equations effected by viscosity are identical for both the incompressible and compressible analyses the "viscous solutions" should be identical in both cases. It is then readily shown that another independent solution of the disturbance equations is,

$$\begin{aligned} \hat{p} &= 0 \\ \hat{u} &= U_o I_o(\lambda r) \\ \hat{v} &= -U_o \frac{i\alpha}{\lambda} I_1(\lambda r) \end{aligned} \tag{A.23}$$

The same analysis may be applied to any region where the flow is uniform. The solutions for any region in which $\bar{\rho} = \rho_o$ and $\bar{u} = \bar{u}_o$ may be written as:

$\underline{m = 0}$:

$$\hat{p} = A_{1,2} H_o^{(1),(2)}(i\lambda^* r) \tag{A.24}$$

$$\hat{u} = A_{1,2}\frac{\alpha(R - iM_J^2\Omega)}{\rho_o \Omega R} H_o^{(1),(2)}(i\lambda^* r) + A_{3,4} H_o^{(1),(2)}(i\lambda r) \tag{A.25}$$

$$\hat{v} = -A_{1,2}\, i\lambda^* \frac{(R - iM_J^2\Omega)}{\rho_o \Omega R} H_1^{(1),(2)}(i\lambda^* r) - A_{3,4}\frac{i\alpha}{\lambda} H_1^{(1),(2)}(i\lambda r) \tag{A.26}$$

$\underline{m \neq 0}$:

$$\hat{p} = A_{1,2}\frac{\rho_o \Omega R}{\alpha(R - iM_J^2\Omega)} H_m^{(1),(2)}(i\lambda^* r) \tag{A.27}$$

$$\hat{u} = A_{1,2} H_m^{(1),(2)}(i\lambda^* r) + A_{3,4} H_m^{(1),(2)}(i\lambda r) \tag{A.28}$$

$$\hat{v} = -A_{1,2}\frac{i}{\alpha}\frac{d}{dr}\{H_m^{(1),(2)}(i\lambda^* r)\} - A_{3,4}\frac{\alpha}{\lambda}H_{m+1}^{(1),(2)}(i\lambda r) - A_{5,6}\frac{im}{r}H_m^{(1),(2)}(i\lambda r) \quad (A.29)$$

$$\hat{w} = A_{1,2}\frac{m}{\alpha r}H_m^{(1),(2)}(i\lambda^* r) + A_{3,4}\frac{i\alpha}{\lambda}H_{m+1}^{(1),(2)}(i\lambda r) + A_{5,6}\frac{d}{dr}\{H_m^{(1),(2)}(i\lambda r)\} \quad (A.30)$$

where

$$\Omega = \omega - \alpha\bar{u}_o \ , \quad (A.31)$$

and

$$\lambda^{*2} = \frac{\alpha^2 R - i\lambda^2 M_J^2 \Omega}{(R - iM_J^2\Omega)} \ . \quad (A.32)$$

These solutions have been written in a form appropriate to the conditions far from the jet axis. The choice of the Hankel functions of the first or second kind depends on the argument and the satisfaction of the boundary condition at infinity, A.13. Similar forms, in terms of modified Bessel functions may be written for the solutions in the potential core or close to the jet axis.

Appendix B

In equations 36 and 37 the definition of the functions a through f are,

$$a = \frac{r^2}{\omega^2}\epsilon_t\frac{\bar{u}}{\eta_e^4} \ , \quad (B.1)$$

$$b = \frac{1}{\omega}\frac{\partial}{\partial\omega}\left(\frac{r^2}{\omega}\epsilon_t\frac{\bar{u}}{\eta_e^4}\right) + \frac{2\omega}{\eta_e^2}\frac{d\eta_e^2}{dz} \ , \quad (B.2)$$

$$c = \frac{2}{\omega\eta_e^2}\frac{\partial}{\partial\omega}\{\bar{\bar{u}}\bar{\bar{v}}r\} \ , \quad (B.3)$$

$$d = \frac{1}{\omega}\frac{\partial}{\partial\omega}\left(\frac{r^2}{\omega}\frac{\epsilon_t}{\sigma_k}\frac{\bar{u}}{\eta_e^4}\right) + \frac{2\omega}{\eta_e^2}\frac{d\eta_e^2}{dz} \ , \quad (B.4)$$

$$e = -\frac{4C_2 k^{1/2}}{\bar{u}\,\ell} \ , \text{ and} \quad (B.5)$$

$$f = \frac{r^2}{\omega^2}\frac{\bar{u}}{\eta_e^4}\epsilon_t\left(\frac{\partial\bar{u}}{\partial\omega}\right)^2 - \frac{4\phi_o}{\bar{u}} \ . \quad (B.6)$$

The matrices in equation 40 may be written,

$$\underline{X}_i = \begin{vmatrix} A_i & 0 \\ 0 & A_i' \end{vmatrix} \ , \quad \underline{Y}_i = \begin{vmatrix} B_i & 0 \\ 0 & B_i' \end{vmatrix} \ ,$$

$$\underline{Z}_i = \begin{vmatrix} C_i & 0 \\ 0 & C_i' \end{vmatrix} \quad \text{and} \quad \underline{d}_i = (D_i \ , \ D_i')^T \ , \quad (B.7)$$

where

$$A_i^{j+1} = \left\{\frac{2\sigma}{(1+\sigma)\sigma^{2i-1}(h_1)^2}\tilde{a}_i^{j+1} - \frac{\sigma^2}{(1+\sigma)\sigma^i h_1}\tilde{b}_i^{j+1}\right\}\lambda\Delta\zeta \quad (B.8)$$

$$B_i^{j+1} = \left\{-\frac{2}{\sigma^{2i-1}(h_1)^2}\tilde{a}_i^{j+1} + \frac{(\sigma-1)}{\sigma^i h_1}\tilde{b}_i^{j+1}\right\}\lambda\Delta\zeta - 1 \quad (B.9)$$

$$C_i^{j+1} = \left\{\frac{2}{(1+\sigma)\sigma^{2i-1}(h_1)^2}\tilde{a}_i^{j+1} + \frac{1}{(1+\sigma)\sigma^i h_1}\tilde{b}_i^{j+1}\right\}\lambda\Delta\zeta \quad (B.10)$$

$$D_i = -\left\{a_i^j\left(\frac{\partial^2\bar{u}}{\partial\omega^2}\right)_i^j + b_i^j\left(\frac{\partial n}{\partial\omega}\right)_i^j\right\}(1-\lambda)\Delta\zeta - \left\{\lambda\tilde{c}_i^{j+1} + (1-\lambda)c_i^j\right\}\Delta\zeta - \bar{u}_i^j \quad (B.11)$$

$$A_i'^{j+1} = \left\{\frac{2\sigma}{(1+\sigma)\sigma^{2i-1}(h_1)^2}\frac{\tilde{a}_i^{j+1}}{\sigma_k} - \frac{\sigma^2}{(1+\sigma)\sigma^i h_1}d_i^{j+1}\right\}\lambda\Delta\zeta \quad (B.12)$$

$$B_i'^{j+1} = \left\{-\frac{2}{\sigma^{2i-1}(h_1)^2}\frac{\tilde{a}_i^{j+1}}{\sigma_k} + \frac{(\sigma-1)}{\sigma^i h_1}\tilde{d}_i^{j+1} + \tilde{e}_i^{j+1}\right\}\lambda\Delta\zeta - 1 \quad (B.13)$$

$$C_i'^{j+1} = \left\{\frac{2}{(1+\sigma)\sigma^{2i-1}(h_1)^2}\frac{\tilde{a}_i^{j+1}}{\sigma_k} + \frac{1}{(1+\sigma)\sigma^i h_1}\tilde{d}_i^{j+1}\right\}\lambda\Delta\zeta \quad (B.14)$$

$$D_i' = -\left\{\frac{a_i^j}{\sigma_k}\left(\frac{\partial^2 k}{\partial\omega^2}\right)_i^j + d_i^j\left(\frac{\partial k}{\partial\omega}\right)_i^j + e_i^j k_i^j\right\}(1-\lambda)\Delta\zeta - \left\{\lambda\tilde{f}_i^{j+1} + (1-\lambda)f_i^j\right\}\Delta\zeta - k_i^j \ , \quad (B.15)$$

where a tilde denotes the guessed value from a previous iteration.

The boundary conditions on $\bar{u}$ and k may be written,

$$\begin{matrix} \bar{u}_o = \bar{u}_1 & k_o = k_1 \\ \bar{u}_N = 0 & k_N = 0 \end{matrix} \ , \quad (B.16)$$

$$\underline{Y}_o = \underline{Y}_N = \underline{I} \ , \ \underline{Z}_o = -\underline{I} \text{ and } \underline{X}_N = \underline{0} \ , \quad (B.17)$$

where $\underline{I}$ is the identity matrix and $\underline{0}$ is the zero matrix,

and $$\underline{d}_o = (0, 0)^T \ , \ \underline{d}_N = (0, 0)^T \ . \quad (B.18)$$

PSU-AERO-PA-80/81-2

THE VISCOUS STABILITY OF COMPRESSIBLE AXISYMMETRIC JETS

by

Philip J. Morris*

The Pennsylvania State University
University Park, Pa. 16802

---

* Associate Professor, Department of Aerospace Engineering, Member AIAA

Abstract

Calculations of the viscous, spatial stability characteristics of a compressible axisymmetric jet have been made. The asymptotic solutions to the stability equations in regions of constant mean flow properties are developed and used as the boundary conditions for a numerical integration of the compressible stability equations in cylindrical coordinates. Calculations are presented for a range of Mach and Reynolds numbers for both the axisymmetric and helical modes. Increasing the Mach number is found to stabilize the flow as is decreasing the Reynolds number. The helical mode is found to be more unstable than the axisymmetric mode for higher Mach numbers. The viscous calculations are found to closely approach the inviscid limit for local Reynolds numbers greater than 500.

Introduction

The stability characteristics of free shear flows are of considerable interest in the field of aerodynamic noise. Instability waves appear to perform an important role in noise radiation at both subsonic and supersonic mean flow velocities (Moore[1] and McLaughlin, et al.[2]). Analytical studies of noise radiation by instability waves, such as that by Tam and Morris[3] have assumed that because of the dynamic instability of the mean flow profile in jets and shear layers an inviscid analysis may be used. Though this assumption appears justified by comparison with experiment and has the attraction of simplicity it has a disadvantage. For damped waves, though valid inviscid solutions do exist, the solution is not valid over the entire transverse coordinate. If a more detailed analysis of the interaction between the instability wave and the other components of the fluid motion is desired knowledge of the wave properties at all real locations is required. Such interactions are thought to be responsible for the broadband jet noise amplification measured by Bechert and Pfizenmaier[4], Moore[1], and others. The analysis of the present paper overcomes this difficulty by using a viscous analysis. The question of the appropriate choice of Reynolds number in a given flow problem, whether the basic flow is laminar or turbulent, is not addressed. Solutions and calculations are presented for the viscous compressible stability equations in cylindrical coordinates.

The inviscid stability of compressible jet flows has been studied by many authors including Lessen, Fox and Zien[5] and Michalke[6]. The former considered a cylindrical vortex sheet and the latter used realistic mean flow profiles which simulated the initial and final stages of the annular

jet mixing region. The viscous stability of incompressible axisymmetric jet flows with realistic mean velocity profiles has been calculated by Burridge[7], Mollendorf and Gebhart[8], Lessen and Singh[9], and Morris[10]. All authors considered a jet velocity profile given by $u = (1 + r^2)^{-2}$ which is characteristic of the flow downstream of the annular mixing region. Morris[10] also considered the same mean flow profiles used by Michalke.

The present paper describes the viscous stability of a compressible axisymmetric jet to disturbances of arbitrary azimuthal mode number. The asymptotic solutions to the compressible stability equations are developed. Calculations are presented for a range of Mach numbers and Reynolds numbers for a mean velocity profile considered by Michalke[6] and Morris[10] which is characteristic of the end of the annular mixing region of the jet.

The Stability Equations and Boundary Conditions

The full compressible stability equations in Cartesian coordinates have been developed by Lees and Lin[11]. A simpler set of equations which neglect viscous effects in the energy equation was introduced by Dunn and Lin[12]. A similar simplification is used in the present paper. The dissipation terms are neglected in the energy equation and the viscous effects in the momentum equations are characterized by their incompressible form. Variations in the molecular properties of the fluid are also neglected. Though these assumptions restrict the analysis to moderate Mach numbers and flows with little variation in the mean static temperature it should be remembered that the purpose of the analysis is to provide a viscous correction to the inviscid analysis to enable solutions to be obtained along the

real radial axis. With the further assumption that the mean flow properties are functions of the radial coordinate alone, the "parallel-flow approximation," the linearized disturbance equations may be written,

$$M^2\left\{\frac{\partial p'}{\partial t} + \bar{u}\,\frac{\partial p'}{\partial z}\right\} + \Delta' = 0 \tag{1}$$

$$\bar{\rho}\left\{\frac{\partial v'}{\partial t} + \bar{u}\,\frac{\partial v'}{\partial z}\right\} + \frac{\partial p'}{\partial r} = \frac{1}{R}\left\{\nabla^2 v' - \frac{v'}{r^2} - \frac{2}{r^2}\,\frac{\partial w'}{\partial \phi}\right\} \tag{2}$$

$$\bar{\rho}\left\{\frac{\partial w'}{\partial t} + \bar{u}\,\frac{\partial w'}{\partial z}\right\} + \frac{1}{r}\,\frac{\partial p'}{\partial \phi} = \frac{1}{R}\left\{\nabla^2 w' - \frac{w'}{r^2} + \frac{2}{r^2}\,\frac{\partial v'}{\partial \phi}\right\} \tag{3}$$

$$\bar{\rho}\left\{\frac{\partial u'}{\partial t} + \bar{u}\,\frac{\partial u'}{\partial z} + v'\,\frac{d\bar{u}}{dr}\right\} + \frac{\partial p'}{\partial z} = \frac{1}{R}\,\nabla^2 u' \ , \tag{4}$$

where

$$\Delta' = \left\{\frac{1}{r}\,\frac{\partial v' r}{\partial r} + \frac{1}{r}\,\frac{\partial w'}{\partial \phi} + \frac{\partial u'}{\partial z}\right\} \ , \tag{5}$$

The velocity components in the (r, ϕ, z) directions are v, w, and u, respectively, overbars denote the mean flow, and primes denote disturbances. All quantities have been nondimensionalized with respect to the jet exit conditions, e.g. $\bar{u} = u^*/\bar{u}_J$, $r = r^*/r_J$, $p = p^*/\bar{\rho}_J \bar{u}_J^{\,2}$, where stars denote a dimensional quantity and the subscript J denotes jet exit conditions. The Reynolds number and Mach number are given by,

$$R = \bar{\rho}_J \bar{u}_J \bar{r}_J/\bar{\mu}_J \quad \text{and} \quad M = \bar{u}_J/\bar{a}_J \ , \tag{6}$$

where $\bar{a}$ is the local speed of sound. For $R \to \infty$ equations (1)-(4) approach the inviscid system of equations and for $M = 0$ they are the viscous incompressible equations in cylindrical coordinates.

A disturbance is assumed to possess a wavelike form with prescribed azimuthal periodicity such that, for example,

$$u'(r,\phi,z,t) = \mathrm{Re}[\hat{u}(r)\exp\{i(\alpha z - \omega t + n\phi)\}] \tag{7}$$

where α is the complex axial wavenumber, ω is the real radian frequency and n is the azimuthal mode number. Substituting terms of the form (7) for the velocity and pressure fluctuations in equations (1)-(5) yields a system of four coupled ordinary differential equations for the four unknown functions, $\hat{u}(r)$, $\hat{v}(r)$, $\hat{w}(r)$ and $\hat{p}(r)$. These equations may be written,

$$-i\Omega\bar{\rho}\hat{v} + \hat{p}' = \frac{1}{R}\left\{\hat{v}'' + \frac{\hat{v}'}{r} - \left[\alpha^2 + \frac{(n^2+1)}{r^2}\right]\hat{v} - i\,\frac{2n}{r^2}\,\hat{w}\right\} , \tag{8}$$

$$-i\Omega\bar{\rho}\hat{w} + \frac{im}{r}\,\hat{p} = \frac{1}{R}\left\{\hat{w}'' + \frac{\hat{w}'}{r} - \left[\alpha^2 + \frac{(n^2+1)}{r^2}\right]\hat{w} + i\,\frac{2n}{r^2}\,\hat{v}\right\} , \tag{9}$$

$$-i\Omega\bar{\rho}\hat{u} + \bar{\rho}\bar{u}'\hat{v} + i\alpha\hat{p} = \frac{1}{R}\left\{\hat{u}'' + \frac{\hat{u}'}{r} - \left[\alpha^2 + \frac{n^2}{r^2}\right]\hat{u}\right\} , \tag{10}$$

and

$$-iM^2\Omega\hat{p} + \left\{\hat{v}' + \frac{\hat{v}}{r} + \frac{in\hat{w}}{r} + a\alpha\hat{u}\right\} = 0 , \tag{11}$$

where primes denote differentiation with respect to r and,

$$\Omega = \omega - \alpha\bar{u} \tag{12}$$

The boundary conditions on the fluctuations which are kinematic in origin at r = 0 were developed by Batchelor and Gill[13]

$$\begin{aligned}
&\hat{v},\ \hat{w},\ \hat{u},\ \hat{p} \to 0 \quad \text{as} \quad r \to \infty \\
&\hat{u}(0) = \hat{p}(0) = 0 \ , \quad n \neq 0 \ , \\
&\hat{v}(0) = \hat{w}(0) = 0 \ , \quad n \neq 1 \ , \\
&\hat{v}(0) + i\hat{w}(0) = 0 \ , \quad n = 1 \ .
\end{aligned} \tag{13}$$

The numerical solution of equations (8)-(11) depends on a knowledge of the solutions at the edges of the integration region where the mean flow properties are taken to be constant. These asymptotic solutions are developed in the next section.

Asymptotic Solutions

In order to determine the form of the solution in regions of constant mean flow properties a series solution is developed for small r. The form of this solution is found to indicate the general solution of the equations. For n = 0 equation (9) is uncoupled and equations (8), (10), and (11) provide a system for $\hat{u}$, $\hat{v}$, and $\hat{p}$. Since this case is algebraically simpler than that for asymmetric disturbances its solution is given more fully and the corresponding solution for $n \neq 0$ will only be stated.

Consider a region in which $\bar{u} = \bar{u}_o$, $\bar{\rho} = \bar{\rho}_o$ and $\Omega = \Omega_o$ where the subscript o indicates a constant mean flow property. Then equations (8), (10), and (11) reduce to,

$$-i\rho_o\Omega_o\hat{v} + \hat{p}' = \frac{1}{R}\left[\hat{v}'' + \frac{\hat{v}'}{r} - \left(\alpha^2 + \frac{1}{r^2}\right)\hat{v}\right] , \tag{14}$$

$$-i\rho_o\Omega_o\hat{u} + i\alpha\hat{p} = \frac{1}{R}\left[\hat{u}'' + \frac{\hat{u}'}{r} - \alpha^2\hat{u}\right] , \tag{15}$$

and

$$-iM^2\Omega_o\hat{p} + \frac{(\hat{v}r)'}{r} + i\alpha\hat{u} = 0 \tag{16}$$

From the boundary conditions (13) the form of series expansions, for small r, for the dependent variables is found to be,

$$\hat{v} = V_1 r + V_3 r^3 + V_5 r^5 + \text{---}$$
$$\hat{u} = U_o r + U_2 r^2 + U_4 r^4 + \text{---}$$
$$\hat{p} = P_o r + P_2 r^2 + P_4 r^4 + \text{---} \qquad (17)$$

After considerable algebra it is found that

$$\hat{p} = P_o\{1 + \frac{\lambda^{*2} r^2}{4} + \frac{\lambda^{*4} r^4}{64} + \text{---}\} , \qquad (18)$$

where
$$\lambda^{*2} = \frac{(\alpha^2 R - i\lambda^2 M^2 \Omega_o)}{(R - iM^2\Omega_o)} , \qquad (19)$$

and
$$\lambda^2 = \alpha^2 - i\rho_o \Omega_o R . \qquad (20)$$

However, equation (18) is the series expansion for the Modified Bessel function of the first kind, so that,

$$\hat{p} = P_o I_o(\lambda^* r) . \qquad (21)$$

The corresponding forms for $\hat{u}$ and $\hat{v}$ are then readily shown to be,

$$\hat{u} = P_o \, \alpha \frac{(R - iM^2\Omega_o)}{\rho_o \Omega_o R} \; I_o(\lambda^* r) \qquad (22)$$

$$\hat{v} = -P_o \, i\lambda^* \frac{(R - iM^2\Omega_o)}{\rho_o \Omega_o R} \; I_1(\lambda^* r) . \qquad (23)$$

Now equations (14)-(16) are a fourth order system of equations, thus two linearly independent solutions which satisfy the boundary conditions should exist. However, the form for $\hat{p}$ contains only one arbitrary coefficient. This results from $\hat{p}$ only satisfying an "inviscid" equation. The "viscous"

solution for $\hat{p}$ is zero. With $\hat{p} = 0$ in equations (14)-(16) they are identical to the incompressible viscous equations. Thus the "viscous" solutions for the velocity fluctuations are identical to their incompressible form given by Morris[10]. The general solution to the stability equations may now be written down. Their form is given for large r, outside the jet flow, where the Modified Bessel functions are replaced by Hankel functions. The asymptotic solutions are,

<u>n = 0</u>

$$\hat{p} = A_1 H_o^{(1)} (i\lambda^* r) , \tag{24}$$

$$\hat{u} = A_1 \frac{\alpha(R - iM^2\Omega_o)}{\rho_o \Omega_o R} H_o^{(1)} (i\lambda^* r) + A_3 H_o^{(1)} (i\lambda r) , \tag{25}$$

$$\hat{v} = -A_1 \, i\lambda^* \frac{(R - iM^2\Omega_o)}{\rho_o \Omega_o R} H_1^{(1)} (i\lambda^* r) - A_3 \frac{i\alpha}{\lambda} H_1^{(1)} (i\lambda r) . \tag{26}$$

<u>n ≠ 0</u>

$$\hat{p} = A_1 \frac{\rho_o \Omega_o R}{\alpha(R - iM^2\Omega)} H_n^{(1)} (i\lambda^* r) \tag{27}$$

$$\hat{u} = A_1 H_n^{(1)} (i\lambda^* r) + A_3 H_n^{(1)} (i\lambda r) \tag{28}$$

$$\hat{v} = -A_1 \frac{i}{\alpha} \frac{d}{dr} \{H_n^{(1)} (i\lambda^* r)\} - A_3 \frac{\alpha}{\lambda} H_{n+1}^{(1)} (i\lambda r) - A_5 \frac{in}{r} H_n^{(1)} (i\lambda r) \tag{29}$$

$$\hat{w} = A_1 \frac{n}{\alpha r} H_n^{(1)} (i\lambda^* r) + A_3 \frac{i\alpha}{\lambda} H_{n+1}^{(1)} (i\lambda r) + A_5 \frac{d}{dr} \{H_n^{(1)} (i\lambda r)\} . \tag{30}$$

The real parts of λ^* and λ are taken to be positive so as to satisfy the outer boundary conditions. Similar forms, in terms of Modified Bessel functions may be written for the solutions in the potential core or very close to the jet axis. It should be noted that for $M = 0$, $\lambda^* = \alpha$ and the viscous incompressible solutions are recovered and for $1/R = 0$, $\lambda^{*2} = \alpha^2 - M^2\Omega_o^2\rho_o$, and the compressible, inviscid solutions are found.

Calculations

Mean Velocity and Temperature Profiles

The mean velocity profile considered in the calculations is representative of jet profiles towards the end of the potential core. The same profile has been used by Michalke[6] and Morris[10]. The velocity profile may be written as,

$$\bar{u} = \frac{1}{2}\left\{1 + \tanh\left[\frac{1}{4\theta}\left(\frac{1}{r} - r\right)\right]\right\} , \tag{31}$$

where θ is the local momentum thickness and its variation was used by Michalke[10] to represent the influence of axisymmetry on the jet stability. The mean density in the jet is related to the velocity using a Crocco relationship of the form,

$$\bar{\rho} = T^*/\left\{1 + (T^* - 1)\bar{u} + \frac{1}{2}(\gamma - 1)\, M^2 T^*\, \bar{u}(1 - \bar{u})\right\} , \tag{32}$$

which is identical to the form used by Michalke[10] except that T^* is defined as the jet static temperature ratio,

$$T^* = T_J/T_o , \tag{33}$$

where T_o is the ambient temperature.

Numerical Procedure

Calculations have been performed for $\theta = 0.16$. The numerical solution is started at $r = 4.0848$ where $\bar{u} = 6.0 \times 10^{-6}$ using the linearly independent solutions given by equations (24)-(30). The stability equations are integrated numerically using a fixed step-size Runge-Kutta integrator with the linear independence of the solutions being preserved by an orthonormalization procedure. The numerical integration is stopped at $r = 0.2448$, where $\bar{u} = 0.99999$ and the numerical solutions are matched with the known form of the solutions in the potential core. This matching procedure leads to a determinant whose magnitude must be minimized to obtain the eigensolution. An iterative technique based on an inverse Lagrangian interpolation procedure is used to determine an eigenvalue. Further details of the numerical procedure are given by Morris[10]. The inviscid calculations, which are shown for comparison were obtained by solving the second order ordinary differential equation for the pressure on the same integration contour.

Results

In spite of the large number of parameters that enter the problem in compressible viscous analyses only a limited number of calculations are presented. The trends that were previously observed in the limiting cases, inviscid compressible flow and viscous incompressible flow, are also found in the present results. All calculations have been performed for a jet static temperature ratio, $T^* = 1.0$.

Effect of Mach Number. The variation of the local growth rate, $-\alpha_i\theta$, for the axisymmetric, n = 0, mode and the asymmetric, n = 1, mode, are shown in Figures 1 and 2, respectively. Also shown is the inviscid solution for M = 0. The results are for a local Reynolds number, $R\theta = 80$. In both cases as the Mach number increases so the maximum growth rate decreases and the range of amplifying frequencies decreases. The more rapid decrease in amplification rate with Mach number is for the n = 0 mode. This indicates that for higher Mach numbers the n = 1 mode will be more likely to occur naturally. This was observed in the measurements of McLaughlin et al.[2]. The frequency for maximum growth rate decreases with increasing Mach number for both modes but is lower for the n = 1 mode. The variation of the phase velocity, given by ω/α_r, is shown in Figures 3 and 4 for the n = 0 and n = 1 modes, respectively. At low frequencies the phase velocity for the n = 0 mode is greater than the jet centerline velocity. Increasing the Mach number results in a decrease in the phase velocity for most of the amplifying frequencies. At high frequencies where the disturbances are damped increasing the Mach number results in a slight increase in phase velocity. The variation of the phase velocity with Mach number is much less for the n = 1 mode, the phase velocity being approximately 0.6 times the jet centerline velocity for all except the lowest frequencies. The variation of maximum growth rate and phase velocity at the frequency for maximum growth for the two modes is given in Table 1. In spite of the wide variation in phase velocity for different frequencies for the n = 0 mode its phase velocity at the frequency for maximum amplification is virtually independent of Mach number.

Effect of Reynolds Number. The variations with Reynolds number and frequency of the local growth rate, $-\alpha_i\theta$, for the n = 0 and n = 1 modes are shown in Figures 5 and 6, respectively. The results are for a Mach number of 1.0. The inviscid result at this Mach number is also shown. The trends are the same as those calculated by Morris[10] for the incompressible case. Increasing the Reynolds number increases the growth rate at all frequencies. Calculations have not been performed for damped disturbances with supersonic phase velocities. The existence of these modes has been questioned by Lessen et al.[14] and even if they exist physically it appears that the present formulations of stability theory are inadequate for their correct treatment. There is little variation with Reynolds number of the phase velocities for either the n = 0 or n = 1 mode. This is shown in Figure 7 where the growth rates and phase velocities, relative to the inviscid values, are shown for both modes as a function of Reynolds number for a fixed frequency, $\omega\theta = 0.14$, which is close to the maximum amplification frequency for the n = 0 mode. For $\omega\theta = 0.14$ and M = 1.0, the local growth rate in the inviscid limit for the n = 0 mode is $-\alpha_i\theta = 0.0372$ and the phase velocity is 0.7150. For the n = 1 mode $-\alpha_i\theta = 0.0458$ and the phase velocity is 0.5993. At a local Reynolds number $R\theta = 640$ the viscous growth rate is 96 percent of the inviscid value for the n = 0 mode and 97 percent of the inviscid value for the n = 1 mode. It is clear that the inviscid stability characteristics are recovered for any appropriate "local" Reynolds number greater than, say, 500.0. At lower frequencies the inviscid limit will be approached more slowly since it is the factor (αR) that enters the equations. Thus for lower frequencies a higher value of Reynolds number is required to come close to the inviscid solutions.

Conclusions

Calculations have been presented for the viscous stability characteristics of compressible axisymmetric jets. Asymptotic solutions to the compressible stability equations have been obtained and have been used as boundary conditions for the numerical integration. Increasing the jet Mach number is found to be stabilizing as is decreasing the Reynolds number. The helical, $n = 1$, mode, is more unstable than the axisymmetric, $n = 0$, mode at high Mach numbers. The viscous calculations have been found to approach the inviscid limit for local Reynolds numbers greater than 500.

A number of simplifying assumptions have been made in the development of the compressible stability equations. Extension of the method presented here to a system of equations which includes such effects as temperature dependent molecular properties appears reasonable. However, if the Reynolds number is based on an eddy viscosity the present system of equations appears adequate.

Acknowledgment

This work was supported by the NASA Langley Research Center under Grant NSG 1580. The technical monitor is Dr. T. B. Gatski.

References

[1] Moore, C. J., "The Role of Shear Layer Instability Waves in Jet Exhaust Noise," Journal of Fluid Mechanics, Vol. 80, Pt. 2, 1977, pp. 321-367.

[2] McLaughlin, D. K., Morrison, G. L., and Troutt, R. R., "Experiments on the Instability Waves in a Supersonic Jet and Their Acoustic Radiation," Journal of Fluid Mechanics, Vol. 69, Pt. 1, 1975, pp. 73-95.

[3] Tam, C. K. W. and Morris, P. J., "The Radiation of Sound by the Instability Waves of a Compressible Plane Turbulent Shear Layer," Journal of Fluid Mechanics, Vol. 98, Pt. 2, 1980, pp. 349-381.

[4] Bechert, D. and Pfizenmaier, E., "On the Amplification of Broadband Jet Noise by a Pure Tone Excitation," AIAA Paper 76-489, July 1976.

[5] Lessen, M., Fox, J. A., and Zien, H. M., "The Instability of Inviscid Jets and Wakes in Compressible Fluid," Journal of Fluid Mechanics, Vol. 21, Pt. 1, 1965, pp. 129-143.

[6] Michalke, A., "Instabilität eines kompressiblen runden Freistrahls unter Berücksichtigung des Einflusses der Strahlgrenzschichtdicke," Z. Flugwiss, Vol. 19, 1971, pp. 319-328.

[7] Burridge, D. M., "The Stability of Round Jets," Ph.D. Thesis, Bristol University, 1968.

[8] Mollendorf, J. C. and Gebhart, B., "An Experimental and Numerical Study of the Viscous Stability of a Round Laminar Vertical Jet With and Without Thermal Buoyancy for Symmetric and Asymmetric Disturbances," Journal of Fluid Mechanics, Vol. 61, Pt. 2, 1973, pp. 367-399.

[9] Lessen, M. and Singh, P. J., "The Stability of Axisymmetric Free Shear Layers," Journal of Fluid Mechanics, Vol. 60, Pt. 3, 1973, pp. 433-457.

[10] Morris, P. J., "The Spatial Viscous Instability of Axisymmetric Jets," Journal of Fluid Mechanics, Vol. 77, Pt. 3, 1976, pp. 511-529.

[11] Lees, L. and Lin, C. C., "Investigation of the Stability of the Laminar Boundary Layer in a Compressible Fluid," NACA Tech. Note No. 1115, 1946.

[12] Dunn, D. W. and Lin, C. C., "On the Stability of the Laminar Boundary Layer in a Compressible Fluid," Journal of the Aeronautical Sciences, Vol. 22, 1955, pp. 455-477.

[13] Batchelor, G. K. and Gill, A. E., "Analysis of the Stability of Axisymmetric Jets," Journal of Fluid Mechanics, Vol. 14, Pt. 4, 1962, pp. 529-551.

[14] Lessen, M., Fox, J. A., and Zien, H. M., "Stability of the Laminar Mixing of Two Parallel Streams with Respect to Supersonic Disturbances," Journal of Fluid Mechanics, Vol. 25, Pt. 4, 1966, pp. 737-742.

Table 1. Variation of maximum amplification rate and phase velocity at the maximum amplifying frequency with Mach number, $R\theta = 80$.

	n = 0			n = 1		
M	max. amplifying frequency, $\omega\theta$	$-\alpha_i\theta$	ω/α_r	max. amplifying frequency, $\omega\theta$	$-\alpha_i\theta$	ω/α_r
0	0.1698	0.0490	0.7226	0.1278	0.0515	0.6051
0.4	0.1638	0.0454	0.7230	0.1236	0.0497	0.6021
0.8	0.1474	0.0351	0.7224	0.1110	0.0447	0.5930
1.0	0.1348	0.0278	0.7228	0.1026	0.0413	0.5862
1.2	0.1201	0.0188	0.7225	0.0928	0.0375	0.5780

Figure Captions

Fig. 1 Effect of Mach number on the variation of amplification factor with frequency. $n = 0$, $R\theta = 80.0$. $M = 0$, — — — —; $M = 0.4$, — —— —; $M = 0.8$, – – ——; $M = 1.0$, ·····; $M = 1.2$, – ——– . Inviscid solution, $M = 0$, ————.

Fig. 2 Effect of Mach number on the variation of amplification factor with frequency. $n = 1$, $R\theta = 80.0$. For legend see Fig. 1.

Fig. 3 Effect of Mach number on the variation of phase velocity with frequency. $n = 0$, $R\theta = 80.0$. For legend see Fig. 1

Fig. 4 Effect of Mach number on the variation of phase velocity with frequency. $n = 1$, $R\theta = 80.0$. For legend see Fig. 1.

Fig. 5 Effect of Reynolds number on the variation of amplification factor with frequency. $n = 0$, $M = 1.0$. $R\theta = 20.0$, – ——– ; $R\theta = 40.0$, ·····; $R\theta = 80.0$, – – ——; $R\theta = 160.0$, — —— — ; $R\theta = 320.0$, – – – – – . Inviscid solution, $M = 1.0$, ————.

Fig. 6 Effect of Reynolds number on the variation of amplification factor with frequency. $n = 1$, $M = 1.0$. For legend see Fig. 5.

Fig. 7 Variation of viscous solutions with Reynolds number $(-\alpha_i)/(-\alpha_i)_{inviscid}$, $n = 0$, – – ——; $n = 1$, ————. $(\alpha_r)_{inviscid}/(\alpha_r)$, $n = 0$, – ——– ; $n = 1$, ·····. $M = 1.0$, $\omega\theta = 0.14$.

P. J. Morris
Fig. 1

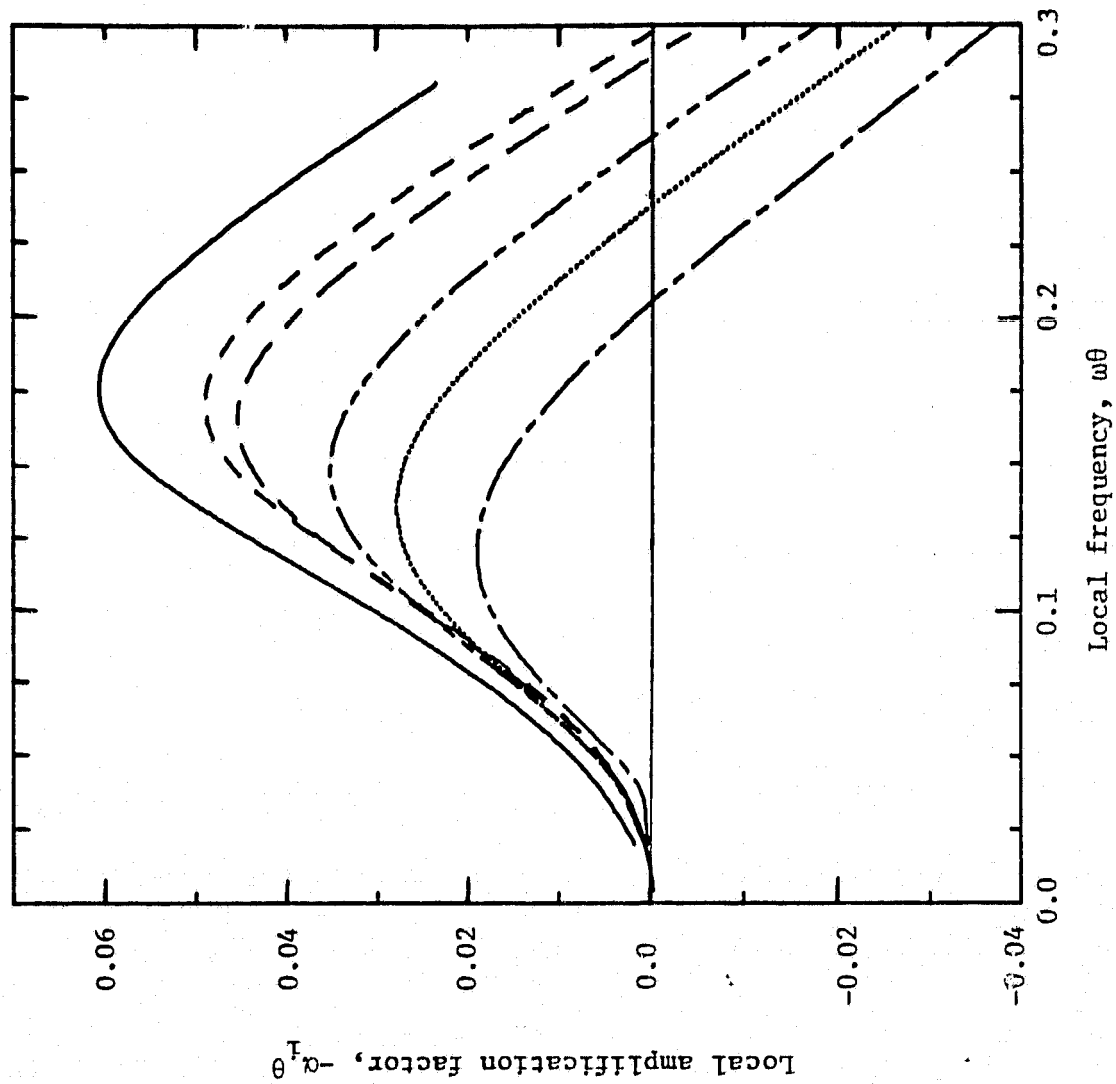

P. J. Morris
Fig. 2

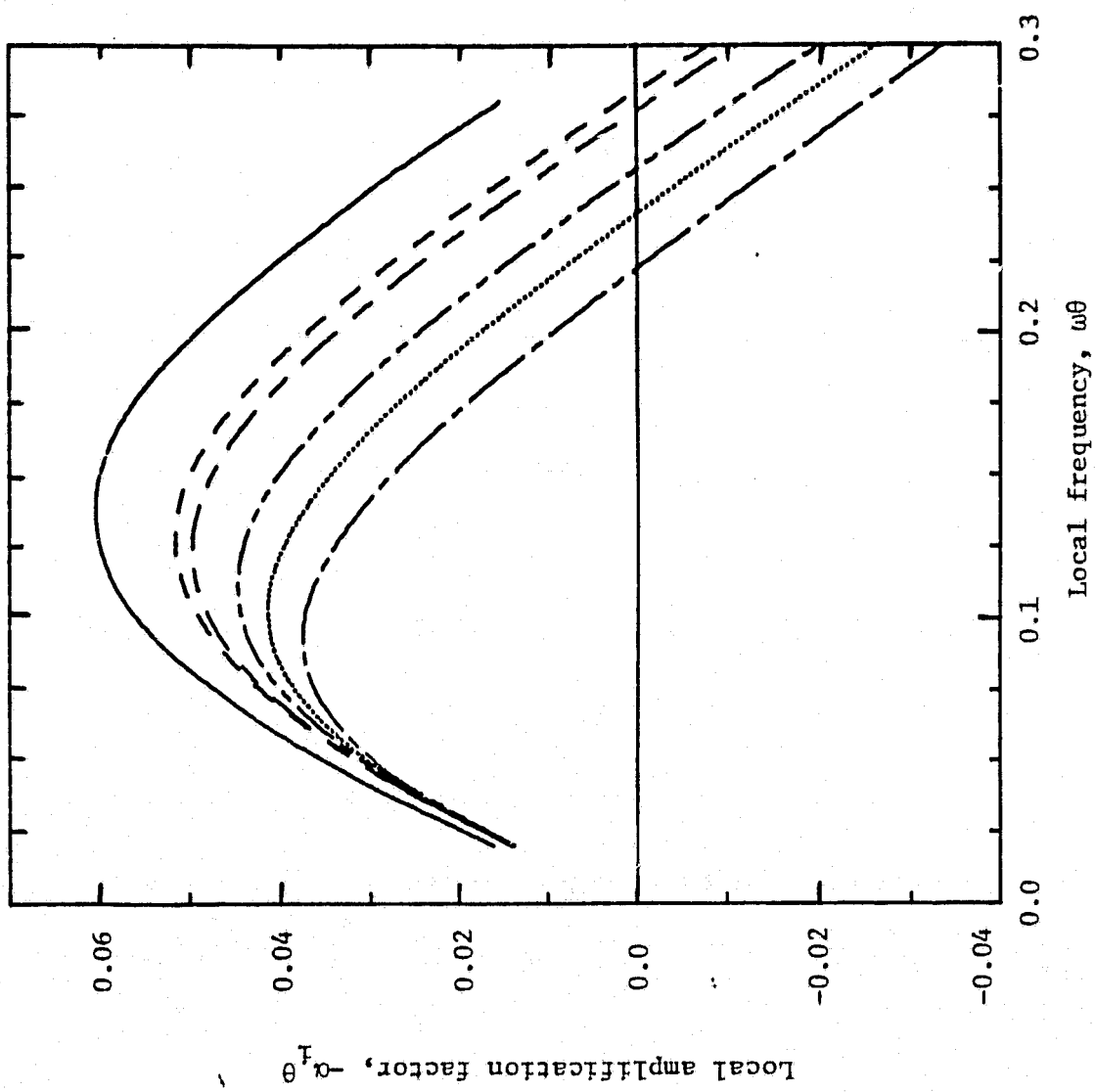

P. J. Morris
Fig. 3

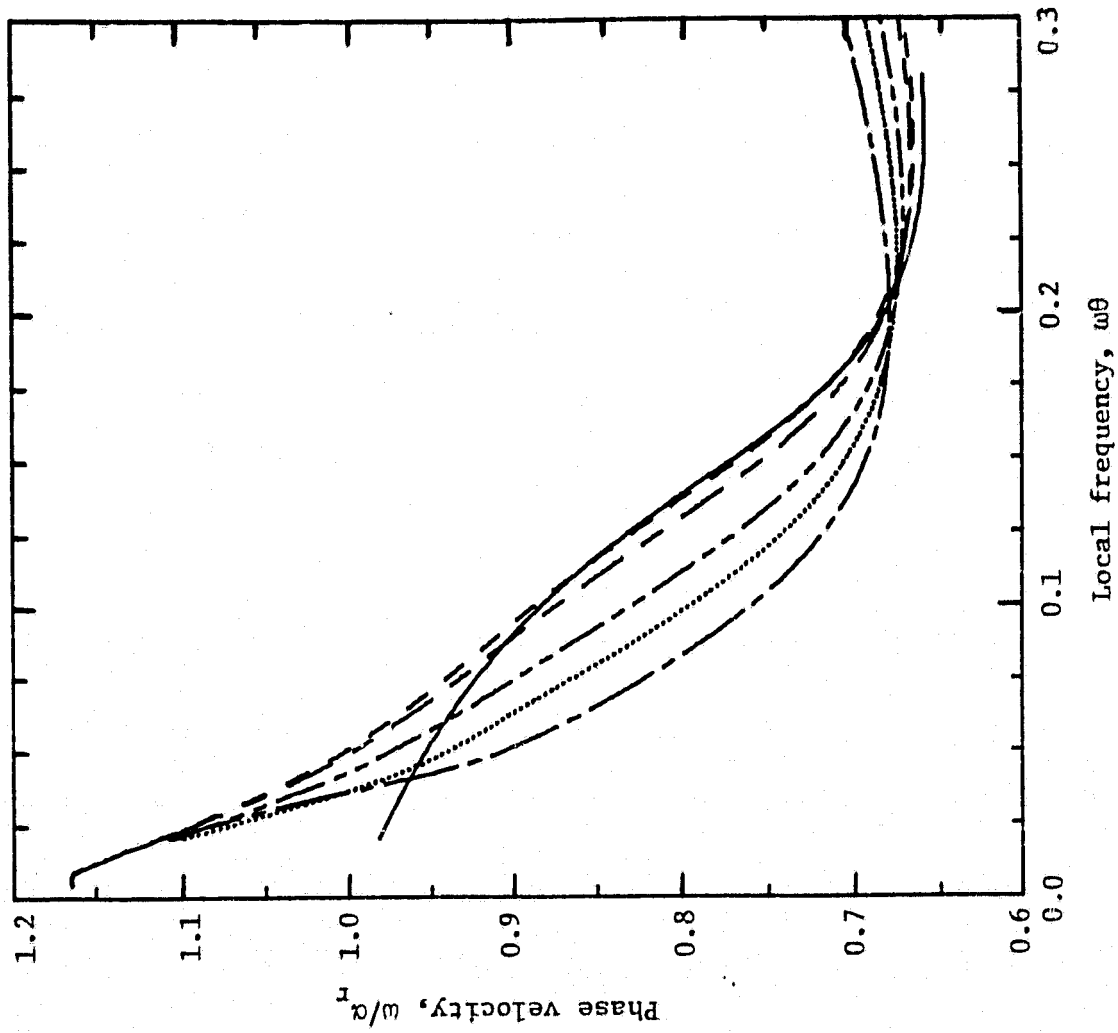

P. J. Morris
Fig. 4

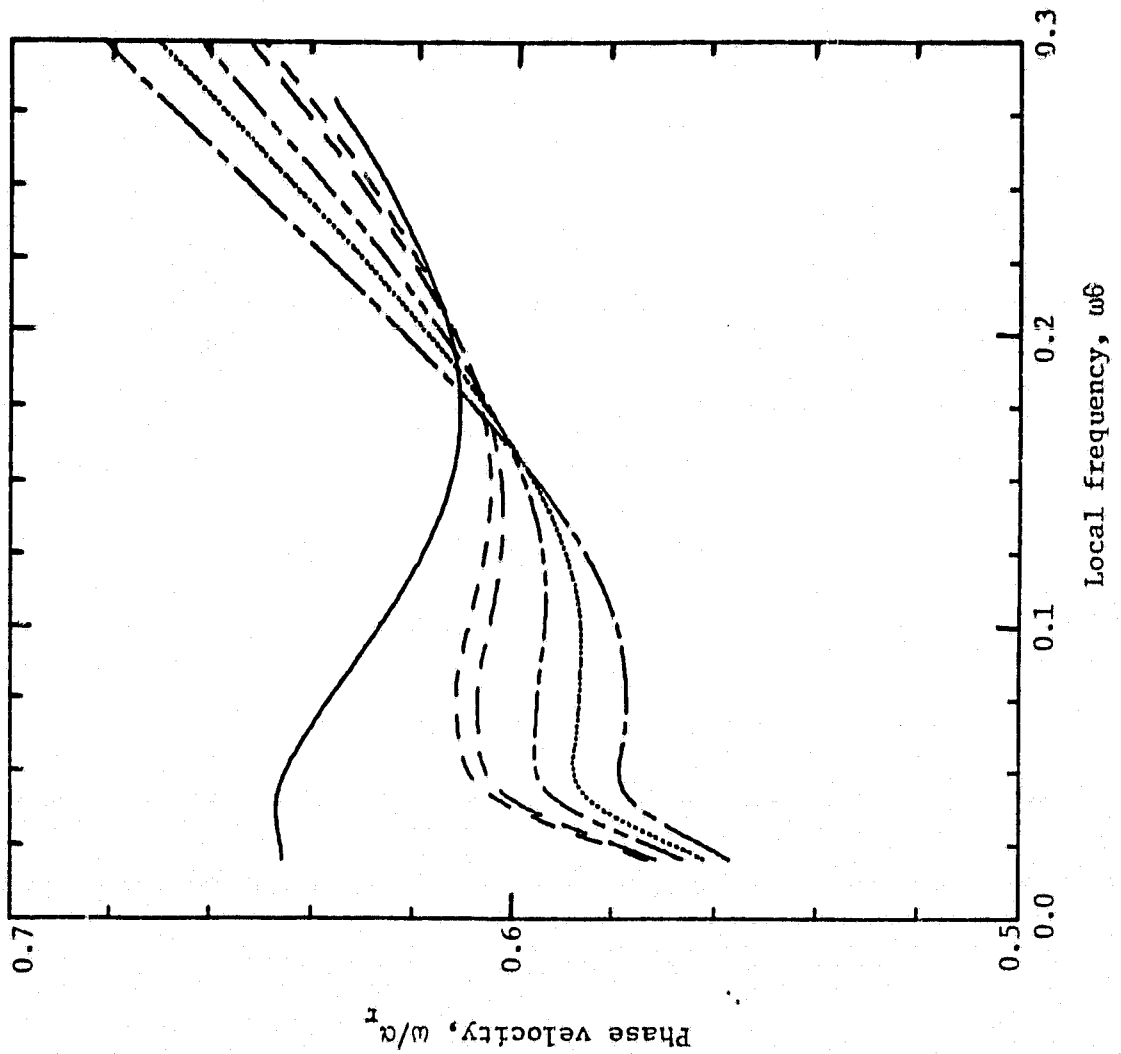

P. J. Morris
Fig. 5

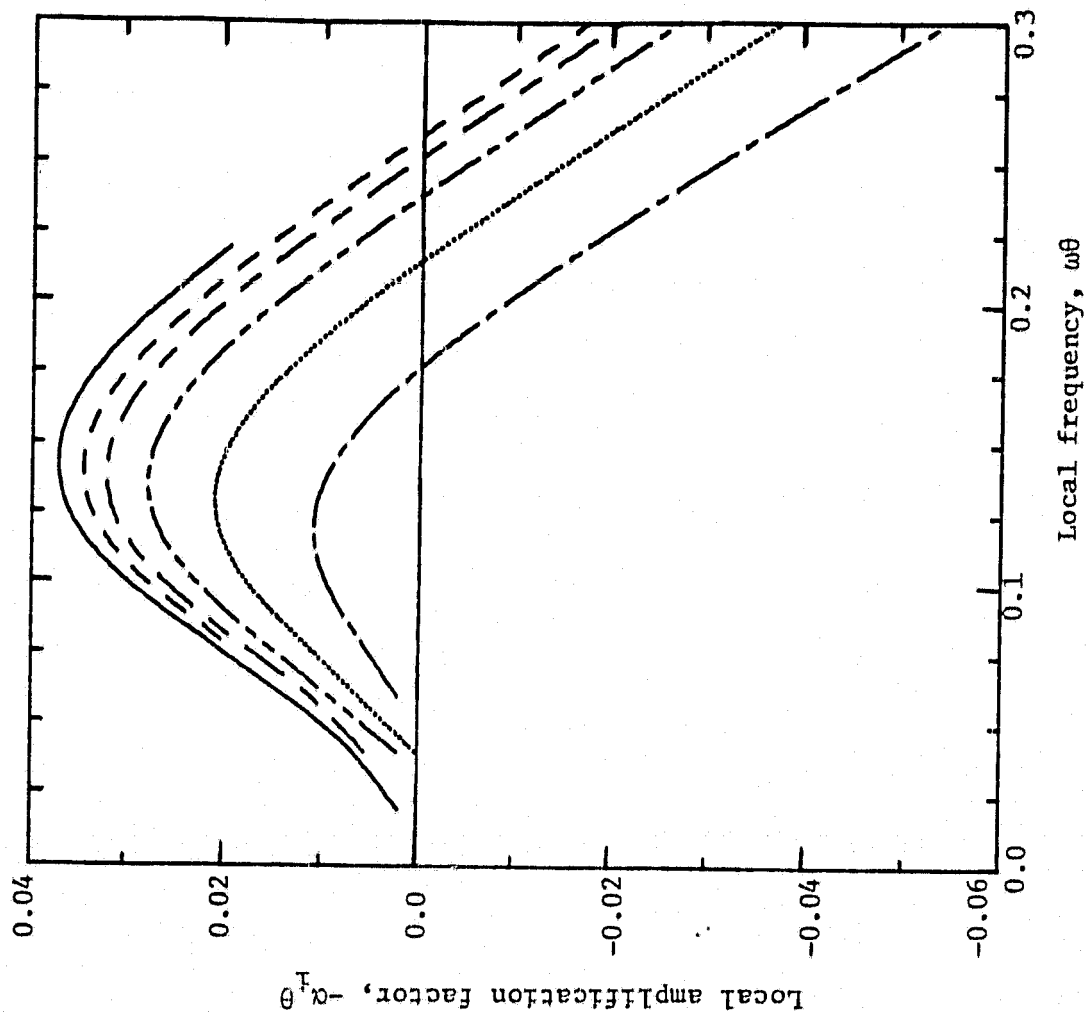

P. J. Morris
Fig. 6

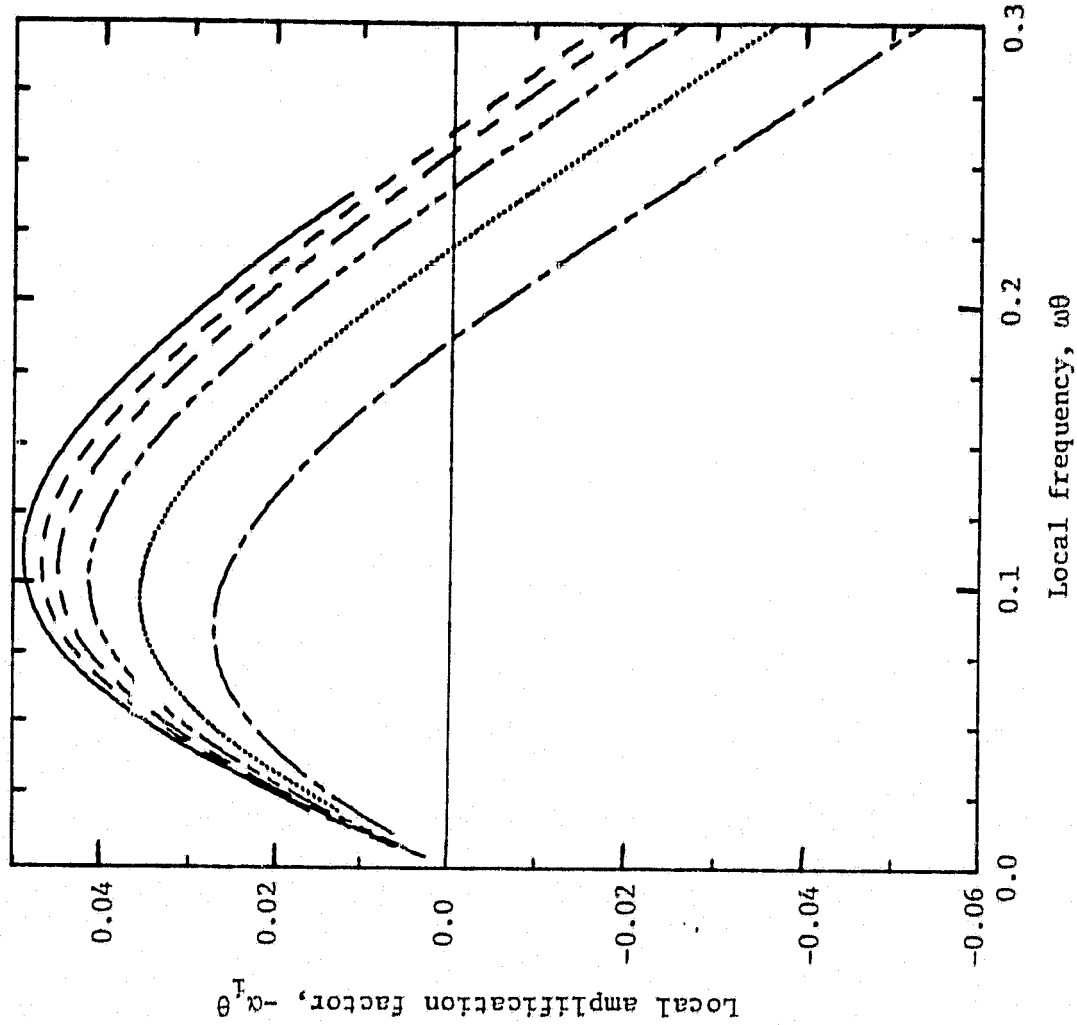

P. J. Morris
Fig. 7